

Exact solutions to planar emittance growth problemsB. Zerbe^{1, a)} and P. M. Duxbury^{1, b)}*Department of Physics and Astronomy, Michigan State University*

(Dated: 2 June 2020)

This paper is the first in a series which develops the theory of emittance dynamics based on simple statistical reasoning. Emittance is a central quantity used to characterize the quality of electron microscopes, photon sources and particle beams. Emittance growth in high intensity charged particle beams is a particularly challenging non-equilibrium statistical physics problem in which effects such as disordered-induced heating and charge reorganization can lead to very rapid degradation of emittance and beam quality. The concepts of free energy and entropy have been utilized to improve conceptual understanding of emittance dynamics. Here we develop a theory based on the second order cumulant of particle distributions and use this formulation to exactly solve several one dimensional problems. These solutions are important extensions of the existing results for the free expansion dynamics of pancake bunches used in ultrafast electron microscopy, which at short times are known to expand quadratically with time¹⁻³. Here we show that the squared emittance of a strictly planar expanding bunch increases as a quadratic polynomial of time. We compare theories based on individual particle trajectories with theories based on distributions and expand the foundations of theories based on individual particle trajectories, which we call the “sample picture”. Our later work uses this formulation to derive generalized envelope equations which capture emittance growth effects in two and three dimensional systems.

^{a)}Electronic mail: zerbe@msu.edu

^{b)}Electronic mail: duxbury@msu.edu

I. INTRODUCTION

Non-equilibrium, and especially non-linear non-equilibrium, systems, are a central problem in modern theory. A significant portion of modern theory focuses on the evolution of the phase-space distribution of particles, and these approaches are generally theoretically grounded in Liouville's theorem that states that the phase-space distribution function is constant along the trajectory of the system. The most central methods in near-equilibrium and non-equilibrium statistical mechanics, including linear response theory, Boltzmann Transport Theory, and the Bogoliubov-Born-Green-Kirkwood-Yvon hierarchy, are based on such approaches, and numerous insights have been obtained from the application of such models [see e.g. textbooks such as Huang, "Statistical Mechanics"⁴ or Kardar "Statistical Physics of Particles"⁵]. Though the phase space distribution is often the central quantity, theories based on particle trajectories are also standard, particularly in computational approaches such as molecular dynamics simulations. Here we show that when the flow of a particle bunch is laminar, or close to laminar, it is possible to develop analytic theories for particle trajectories which can be used to develop theories for the dynamics of the emittance; as well as for the expansion energy and the energy spread of the beam. This is important as high intensity beams of practical interest are close to laminar.

The discussion of particle beams is often based on continuous distribution functions in $2D$, $6D$, or $6ND$ phase-space. While the descriptions of the evolution of the full distribution function is a common goal of traditional analytic techniques, specific problems often focus on understanding the evolution of specific cumulants, e.g. means and covariances of these distributions. Furthermore the characteristic function, which can be expanded in terms of cumulants or modes, can be thought of as an equivalent description of the phase space distribution albeit in a Fourier-transformed space⁶. Thus the understanding of the moments or cumulants may provide adequate understanding of the distribution without having a full description.

Statistical emittance, henceforth called emittance, is a statistical measure of the quality of an ensemble of particles. It is central to the discussion of numerous bunch phenomena in the accelerator literature⁷⁻¹⁰, and optimizing the emittance is a goal of a large portion of the accelerator community^{8,11}. This measure is obtained from the second order cumulants^{12,13}, and this formulation can be thought of as the square root of the determinant of the covariance

matrix⁸. In the statistics literature, the determinant of the covariance matrix is sometimes referred to as the generalized variance, whose square root can be thought of as a generalized width (area, volume, etc.) in higher dimensions¹⁴. Therefore, emittance can be thought of as an operationalization of phase space area (or volume if in $6D$), and accelerator physicists are specifically interested in the evolution of this measure as well as the covariance measures from which it is derived.

The prevailing energy theory for emittance growth was principally developed in the 70's and 80's. The connection between emittance growth and the field energy contained in an ensemble is largely attributed to Lapostolle¹² and was formalized under the assumption that the field felt at a specific location was identical to the mean-field at that location and that non-linearities in this field led to a free energy that could be thermalized within the beam^{15–17}. Furthermore, Anderson described exact solutions for emittance growth of some simple symmetric models in the presence of a focussing force¹⁸ of note analytically replicating the quarter plasma period emittance explosion seen in simulation by Wangler et. al¹⁵. These ideas were extended by Struckmeier to include Fokker-Planck stochastic effects^{19,20}. These theories paved the way for models explaining beam halo formation^{21,22} and emittance compensation^{23,24}. We note that these theories generally assume continuous, cylindrical-symmetric beam conditions in the presence of a constant focussing force.

Concurrent with the development of this energy theory of emittance growth, Lawson, Lapostolle, and Gluckstern argued that there is a close relation between the entropy and emittance of a beam²⁵. While this idea largely remained dormant until the energy theory was worked out, it was reintroduced in the early 90's^{11,17} to address some issues not answered by the energy theory, and this entropy interpretation gained some popularity, e.g.^{26–31}. However both the energy and the entropy theories have been criticized as phenomenological as they lack any understanding of the mechanism or time dependence of emittance growth, and further that the application of thermodynamic language is largely counterproductive³².

Fundamental to all treatments, though, are the KV envelope equations initially derived through the identification of a very special $6D$ phase space distribution whose projection to any $2D$ phase space is uniform³³. Sacherer presented a derivation of the KV envelope equations through the derivatives of the ensemble cumulants¹³. A subtle definition in Sacherer's work was a statistical definition of the envelope whereas previous work³³ and even some more recent work, e.g.¹⁹, use a more radial-like parameter for the envelope; we will maintain

the statistical definition in this work. Moreover, these envelope equations can be shown to be equivalent to the more recent Analytic Gaussian (AG) equation derived by different means^{34–36}. Sacherer correctly argued that his derivation was more general than Kapchinsky and Vladimirsky’s derivation as it was an approximation of the bunch no matter the underlying phase-space distribution and that the envelope equations predict the evolution of high intensity beams astoundingly well if the emittance dynamics is known *a priori*¹³. In some applications assumption of conserved emittance is a good approximation, however we are most interested in situations where this is not the case. Below we use the term envelope equations to refer to either KV or AG equations.

While the envelope equations are used in essentially all theoretical investigations, their derivation from distribution theory is different than from the sample perspective. It is not clear whether Sacherer understood this difference; specifically, the operator used in his definition of the statistics based on distribution theory enables the commutation of the average and the time derivative operations, which is only true in the distribution theory when collisions are neglected. An important advantage of the sample perspective is that commutation of average and time derivative is exactly true. In the field of statistics, the distinction between analyzing abstract, often continuous distributions and analyzing specific, discrete distributions is distinguished by the terms population and sample statistics³⁷, respectively. Using this vernacular, the standard Liouville theorem distribution-based approaches may be thought of as a population theory whereas theories based on the statistics of individual, particle motion can be thought of as a sample theory. While both notations appear in the literature, they are generally treated as equivalent with no discussion of their differences. We will call the development of a theory that emphasizes the statistical analysis of a single ensemble of particles before applying any population-level insight the sample (statistics) perspective, we will refer to all direct analysis of the phase space distribution as the population (statistic) perspective, and we will highlight some of the theoretical differences that arise when adopting these different perspectives. We develop the sample perspective to garner insight into the mechanisms underlying emittance growth as we argued above that such insight is largely absent from the population perspective. We also note that the sample statistic approach leads naturally to analysis of finite size effects in non-equilibrium systems.

The sample perspective benefits greatly from the Lagrangian description of fluid dynamics. Previous work describing Coulomb explosion^{2,3,38,39} has successfully employed the

Lagrangian description to describe the density evolution from a population perspective. Fundamental to these treatments is the identification of a map from a distribution particle's original position and momentum at some time to its position and momentum at some later time. Within the sample perspective, if the statistics of this map are analyzed, we can obtain deterministic equations for the evolution of the emittance and other measures of beam quality. In fact, this is precisely the approach employed by Sacherer¹³ before deriving his form of the envelope equations. We will explore Sacherer's map later in this manuscript.

The paper is organized as follows. In Section II, we first present the statistics of the sample perspective and contrast it with the population perspective. While these two perspectives are utilized as a matter of course in many areas of research such as stochastic differential equations and statistical physics, the theoretical accelerator physics literature generally focuses on the population perspective; while here we focus on the sample perspective and note how it differs from the population perspective. Section III A describes simple, exact, mathematical relations between sample statistics and key accelerator physics measures of beam quality, such as emittance, when a map between the initial phase coordinates and the phase coordinates at time t can be written. In Section III B we show how these rules can be applied in the non-interacting case leading to an extremely simple interpretation on the importance of the emittance. This analysis is general and may be applied to massless particles and to massive particle beams at any energy. In Section III C we employ sample theory to derive an exact equation for emittance growth in laminar planar models for charged particle beams where the force on each particle can be treated as a constant. This case describes the exact evolution of the statistics of a planar symmetric laminar system under Coulomb repulsion, and by the term exact, we mean that given an exact measurement of the statistics at the initial time, the statistics such as emittance may be determined for all time. We then validate this expression, show that it provides a good approximation even for some non-laminar cases, and further suggest modifications to the theory that should capture the non-laminar case exactly. Up to that point, we will have discussed the exact solution of evolution of the second order statistics; however, the expected solution of the evolution of the statistics can also be obtained from an initial particle distribution. This case is typical of experiments, where the initial phase space distribution may be known, for example a Gaussian particle distribution in the case of photo-injectors used in many electron beam systems^{40–43}. In Section IV A we show how to use arbitrary population distributions to obtain expectations for the emittance

growth using the results of Section III C 1. We then validate these expectations by drawing and evolving multiple N -particle ensembles from three different initial distributions: uniform (Section IV B), Gaussian (Section IV C), and quadratic bimodal (Section IV D). These results show that the expectation of key statistics largely captures the emittance growth of the non-uniform distributions, and that the remainder, or finite system variations, of the emittance growth in all cases is proportional to $\frac{1}{\sqrt{M}}$, where M represents the number of macroparticles, suggesting that its origin is stochastic. In Section V, we show how kinetic energy is naturally written in the sample perspective, and we show how the dynamics of the parameters introduced in previous sections can be used to understand the accounting of energy flow through various modes and how this relates to emittance change. We use this understanding to briefly examine disorder induced heating within the sample perspective. In Section VI we return to the comparison between the population and sample perspectives, discuss some of the more subtle points, and emphasize caveats of using the sample perspective. Finally, in VII, we summarize the main findings of the paper and propose further work that is needed to make this perspective relevant to many key unresolved issues in accelerator physics.

II. THE POPULATION AND SAMPLE PERSPECTIVES

We begin with the standard formulation of the non-equilibrium theory relevant to the accelerator physics field with special attention to the role of collisions and the first and second order cumulants of the distribution. Central to the theory is the continuous $6ND$ phase space distribution at time t , $f_{6ND}(\vec{x}_1, \vec{x}_2, \dots, \vec{x}_N, \vec{p}_1, \vec{p}_2, \dots, \vec{p}_N; t)$. In $6ND$ space, Liouville's theorem applies and $f_{6ND}(\vec{x}_1, \vec{x}_2, \dots, \vec{x}_N, \vec{p}_1, \vec{p}_2, \dots, \vec{p}_N; t) = f_{6ND}(\vec{x}_1, \vec{x}_2, \dots, \vec{x}_N, \vec{p}_1, \vec{p}_2, \dots, \vec{p}_N; 0)$. However, due to the complications with working with $6ND$ space, most work confines itself to presentations of the more workable $6D$ distribution, $f_{6D}(x, y, z, p_x, p_y, p_z; t)$, by introducing a collision term

$$\frac{df_{6D}}{dt} = C(\vec{x}; t) \quad (1)$$

for the time evolution of the distribution — an equation commonly known as the Boltzmann transport equation (BTE). If $C(\vec{x}; t) = 0$ in the BTE — the resulting equation is often called the Vlasov equation — where the $6D$ phase space density function is conserved like

its $6ND$ counterpart. Otherwise, a second function is introduced, $f_{6D,\Delta}(x, y, z, p_x, p_y, p_z; t)$, that accounts for the collision term. Namely

$$f_{6D}(x, y, z, p_x, p_y, p_z; t) = f_{6D}(x, y, z, p_x, p_y, p_z; 0) + f_{6D,\Delta(t)}(x, y, z, p_x, p_y, p_z; t) \quad (2)$$

where $f_{6D}(x, y, z, p_x, p_y, p_z; t)$ has the normalization constraint of $\int_{V_{6D}} f_{6D,\Delta}(x, y, z, p_x, p_y, p_z; t) dV_{6D} = 0$ where V_{6D} represents the entire x, y, z, p_x, p_y, p_z space. It should be obvious that if $C(\vec{x}; t) = 0$ we can write $f_{6D,\Delta}(x, y, z, p_x, p_y, p_z; t) = 0$.

Furthermore, further reduction of the complexity of the phase space is often made by analyzing the marginal distribution integrated over two of the dimension, e.g.

$$f_{2D,x}(x, p_x; t) = \int \int \int \int f_{6D}(\vec{x}, \vec{p}) dp_z dp_y dz dy \quad (3)$$

and analogously for y and z . Assuming the phase space density is not correlated between dimensions, we can write

$$f_{6D}(x, y, z, p_x, p_y, p_z; t) = f_{2D,x}(x, p_x; t) f_{2D,y}(y, p_y; t) f_{2D,z}(z, p_z; t) \quad (4)$$

The expectation of some function of the random variables, $a = a(x, y, z, p_x, p_y, p_z)$, is written as

$$\langle a \rangle = \int_{V_{6D}} a f_{6D} dV_{6D} \quad (5)$$

If $a_x = a_x(x, p_x)$ is only a function of x and p_x and there is no correlation between the dimensions in phase space we have

$$\langle a_x \rangle = \int \int a_x f_{2D,x} dp_x dx \quad (6)$$

which will be the general form of the expectation we examine to simplify the arguments. If $a(x, y, z, p_x, p_y, p_z) = x^i y^j z^k p_x^l p_y^m p_z^n$ for (i, j, k, l, m, n) in the non-negative integers, $\langle a \rangle$ is known as a moment of order $i + j + k + l + m + n$. The 0^{th} order moment is generally set to 1 and is usually called the normalization condition on f_{6D} . Once normalized, all other moments are set by the details of the distribution. Statistics are then functions of these moments, and cumulants can be written in terms of these moments as well. The first order moment and the first cumulant are in fact the same thing.

Of special interest to physics are the covariance statistics. Covariance statistics are defined by

$$\sigma_{a,b} = \langle ab \rangle - \langle a \rangle \langle b \rangle \quad (7)$$

If a and b are linear in x, y, z, p_x, p_y, p_z , these statistics are the second order cumulants. Furthermore, $\sigma_{a,a}$ is usually abbreviated as σ_a^2 , known as the variance of a , so that the standard deviation $\sigma_a = \sqrt{\sigma_{a,a}}$ has a simpler notation. In addition to the σ notation, we will also use $\text{var}(a)$ and $\text{cov}(a, b)$ for σ_a^2 and $\sigma_{a,b}$ when a or b are complicated. Often all relevant second order statistics are put in a 6×6 matrix, called the covariance matrix, whose rows and columns can be thought of as labeled by x, p_x, y, p_y, z, p_z :

$$\mathbf{COV}_{6D} = \begin{bmatrix} \sigma_x^2 & \sigma_{x,p_x} & \sigma_{x,y} & \sigma_{x,p_y} & \sigma_{x,z} & \sigma_{x,p_z} \\ \sigma_{x,p_x} & \sigma_{p_x}^2 & \sigma_{y,p_x} & \sigma_{p_x,p_y} & \sigma_{z,p_x} & \sigma_{p_x,p_z} \\ \sigma_{y,x} & \sigma_{y,p_x} & \sigma_y^2 & \sigma_{y,p_y} & \sigma_{y,z} & \sigma_{y,p_z} \\ \sigma_{x,p_y} & \sigma_{p_x,p_y} & \sigma_{y,p_y} & \sigma_{p_y}^2 & \sigma_{z,p_y} & \sigma_{p_y,p_z} \\ \sigma_{x,z} & \sigma_{z,p_x} & \sigma_{y,z} & \sigma_{z,p_y} & \sigma_z^2 & \sigma_{z,p_z} \\ \sigma_{x,p_z} & \sigma_{p_x,p_z} & \sigma_{y,p_z} & \sigma_{p_y,p_z} & \sigma_{z,p_z} & \sigma_{p_z}^2 \end{bmatrix} \quad (8)$$

Usually \mathbf{COV}_{6D} is assumed to be block diagonal with elements, \mathbf{COV}_x , \mathbf{COV}_y , \mathbf{COV}_z where

$$\mathbf{COV}_x = \begin{bmatrix} \sigma_x^2 & \sigma_{x,p_x} \\ \sigma_{x,p_x} & \sigma_{p_x}^2 \end{bmatrix} \quad (9)$$

and analogously for y and z . Of interest to the accelerator physicist, the $2D$ emittance is defined by

$$\begin{aligned} \epsilon_{x,p_x}^2 &= \frac{1}{m^2 c^2} |\mathbf{COV}_x| \\ &= \frac{1}{m^2 c^2} \text{cov}(x, p_x) \\ &= \frac{1}{m^2 c^2} (\sigma_x^2 \sigma_{p_x}^2 - \sigma_{x,p_x}^2) \end{aligned} \quad (10)$$

where $|\cdot|$ indicates the determinant of the contained matrix. As $\sqrt{|\mathbf{COV}_x|}$ can be thought of as an area of $f_{2D,x}$ in x - p_x space, emittance is often visualized as the area of an ellipse with the appropriate axis lengths determined by the statistics.

The sample perspective is very similar to the population perspective except instead of the continuous $6D$ phase space function, f_{6D} , being central to the definition of the statistics, the discrete N particle sample itself takes this role. Specifically, the mean operator

$$\bar{a} = \frac{1}{N} \sum_{i=1}^N a_i \quad (11)$$

where a_i is the i^{th} value of the random variable a replaces the role of the expectation operator, $\langle \cdot \rangle$. Often \bar{a} is used to estimate the value of $\langle a \rangle$; specifically, it is fairly straightforward to prove

$$\langle \bar{a} \rangle = \langle a \rangle \quad (12)$$

although the exact distribution of a may be of interest to statisticians. However, we emphasize that these population and sample averages are distinct and care needs to be taken when applying equations meant for one to the other.

To keep these operators and the statistics derived from them distinct, we introduce new notation (borrowed from the field of statistics) for the sample covariances. Specifically,

$$s_{a,b} = \overline{ab} - \bar{a}\bar{b} \quad (13)$$

where again a and b are random variables. As is the case for the moments, it is fairly straightforward to show

$$\langle s_{a,b} \rangle = \sigma_{a,b} \quad (14)$$

However, this is not the case for the sample emittance defined by

$$\varepsilon_{x,p_x}^2 = \frac{1}{m^2 c^2} (s_x^2 s_{p_x}^2 - s_{x,p_x}^2) \quad (15)$$

Namely, the expected emittance is

$$\begin{aligned} \langle \varepsilon_{x,p_x}^2 \rangle &= \frac{1}{m^2 c^2} (\langle s_x^2 s_{p_x}^2 \rangle - \langle s_{x,p_x}^2 \rangle) \\ &= \frac{1}{m^2 c^2} (cov(s_x^2, s_{p_x}^2) + \langle s_x^2 \rangle \langle s_{p_x}^2 \rangle \\ &\quad + \langle s_x^2 \rangle \langle s_{p_x}^2 \rangle - var(s_{x,p_x}) - \langle s_{x,p_x} \rangle^2) \\ &= \frac{1}{m^2 c^2} (\sigma_x^2 \sigma_{p_x}^2 - \sigma_{x,p_x}^2 \\ &\quad + cov(s_x^2, s_{p_x}^2) - var(s_{x,p_x})) \\ &= \epsilon_{x,p_x}^2 + \frac{1}{m^2 c^2} (cov(s_x^2, s_{p_x}^2) - var(s_{x,p_x})) \end{aligned} \quad (16)$$

which differs from the population emittance by $\frac{1}{m^2 c^2}(\text{cov}(s_x^2, s_{p_x}^2) - \text{var}(s_{x,p_x}))$.

In addition to this difference in emittance, there is a more fundamental difference between the sample and the population perspectives that arises in the derivative of the operators, which can be thought of as a map relating the statistics at differentially different times. We first derive the differential form in the sample perspective. It is obvious that the time derivative of the mean of a random variable (assuming N is held constant) is,

$$\frac{d}{dt}\bar{a} = \bar{\dot{a}} \quad (17)$$

where \dot{a} is shorthand for $\frac{da}{dt}$. This results in the covariance statistics time derivatives being

$$\frac{d}{dt}s_{a,b} = s_{\dot{a},b} + s_{a,\dot{b}}. \quad (18)$$

This is the map Sacherer used in his derivation of the envelope equations¹³. Here we call Eq. (18) applied to the phase space coordinates the statistical kinematics. Specifically, for the 2D phase space coordinates in the x -direction, the statistical kinematics are

$$\frac{d}{dt}s_x^2 = \frac{2}{m}s_{x,p_x} \quad (19a)$$

$$\frac{d}{dt}s_{x,p_x} = \frac{1}{m}s_{p_x}^2 + s_{x,F_x} \quad (19b)$$

$$\frac{d}{dt}s_{p_x}^2 = 2s_{p_x,F_x} \quad (19c)$$

where $F_x = \frac{dp_x}{dt}$. These equations are exact just as the typical kinematic equations from introductory physics are exact. Furthermore, the time derivate of the sample emittance can be written as

$$\frac{d\epsilon_{x,p_x}^2}{dt} = \frac{2}{m^2 c^2} (s_x^2 s_{p_x,F_x} - s_{x,p_x} s_{x,F_x}) \quad (20)$$

where this equation is again exact.

These statistical kinematic equations can be used to obtain a 2nd order ODE that is the non-relativistic form of Sacherer's envelope equations, by noting that $\frac{d}{dt}s_x^2 = 2s_x \frac{ds_x}{dt}$ where $s_x = \sqrt{s_{x,x}}$. Combining this observation with Eq. (19a) gives

$$\frac{ds_x}{dt} = \frac{1}{m} \frac{s_{x,p_x}}{s_x}, \quad (21)$$

which we will use later. Then taking the derivative of this equation and using Eq. (19b) gives

$$\frac{d^2 s_x}{dt^2} = \frac{1}{m} \frac{s_{x,F_x}}{s_x} + \frac{c^2 \epsilon_{x,p_x}^2}{s_x^3}, \quad (22)$$

Again, this 2^{nd} order ODE is exact meaning that no assumptions or approximations have been made. This equation together with Eq. (20) represents the same degrees of freedom expressed in our statistical kinematics equations (or equivalently the Corant Snyder parameters⁸). The envelope equations can then be obtained by making a single assumption — that F_x is the linear force seen in a uniform ellipsoid, i.e $F_x = \frac{3Ne^2}{40\sqrt{5}\pi\epsilon_0 s_x^3} \alpha\left(\frac{s_y}{s_x}, \frac{s_z}{s_x}\right) x$ where $\alpha(a, b) = \int_0^\infty \frac{1}{(1+\lambda)^{3/2} \sqrt{a^2 + \lambda} \sqrt{b^2 + \lambda}} d\lambda$ giving

$$\frac{d^2 s_x}{dt^2} = \frac{3Ne^2}{40\sqrt{5}\pi m \epsilon_0 s_x^2} \alpha\left(\frac{s_y}{s_x}, \frac{s_z}{s_x}\right) + \frac{c^2 \varepsilon_{x,p_x}^2}{s_x^3}, \quad (23)$$

which is the non-relativistic elliptical envelope equation, which we discuss further in future work. Note that this assumption results in Eq. (20) being 0, which means emittance is conserved; in fact, any assumption of emittance conservation is essentially equivalent to an assumption of the self-force inside the bunch being linear. This means that Sacherer's envelope models¹³ assume such linear forces for a number of non-uniform distributions at least in the approximate sense. Eq. (20) can be ignored and the entire evolution of the statistics can be described by Eq. (23) under such an assumption.

An analogous equation for the time derivative of the population statistics can only be derived if the collision term, $C(\vec{x}; t)$ in Eq. (1), is assumed to be zero. Under such an assumption, we can introduce a map, $\vec{\alpha}(x, y, z, p_x, p_y, p_z, t)$, that is explicitly dependent on time and that relates the Langrangian particle's phase space coordinates at time t to its phase space coordinates at time 0. Another way to state Liouville's theorem is that the phase space is incompressible, so this transformation has a Jacobian of 1. As a result, the expectation of the random variable may be written as

$$\langle a_x \rangle = \int \int a_x(x, p_x, t) f_{6D,x}(x, p_x; 0) dp_x dx \quad (24)$$

Now $f_{2D,x}(x, y, z, p_x, p_y, p_z; 0)$ is no longer dependent on time, but $a_x(x, p_x, t)$ is — that is we have moved the time dependence from $f_{2D,x}$ to the random variable. Thus

$$\frac{d}{dt} \langle a \rangle = \left\langle \frac{da}{d\vec{\alpha}} \frac{d\vec{\alpha}}{dt} \right\rangle \quad (25)$$

Unfortunately, this looks a lot more complicated than it really is — as the statistical reasoning using the population perspective can become fairly abstract and complex. To simplify, a concrete example of this is that

$$\frac{d}{dt} \langle x \rangle = \frac{1}{m} \langle p_x \rangle \quad (26)$$

in the non-relativistic regime. Furthermore, the covariance between a and b for a, b in x, y, z, p_x, p_y, p_z becomes

$$\frac{d}{dt}\sigma_{a,b} = \sigma_{\dot{a},b} + \sigma_{a,\dot{b}} \quad (27)$$

analogous to Eq. (18). Again, though, this is only under the assumption of no collisions, and when collisions are present, this mathematical reasoning fails and generally

$$\frac{d}{dt}\sigma_{a,b} = \sigma_{\dot{a},b} + \sigma_{a,\dot{b}} + C_{a,b}(t) \quad (28)$$

where $C_{a,b}$ accounts for collisions. In other words, Eq. (18) can only be derived in the population perspective if collisions are ignored or if an additional term is added. We note that Kapchinsky and Vladimirovsky made the explicit assumption that their $6D$ phase space volume was conserved meaning that their model was collision-less. It is reasonable to think that Sacherer may have implicitly made the same assumption as he continued to use the population statistics notation; on the other hand, it is equally reasonable to believe that Sacherer thought of the problem from the sample perspective.

In conclusion, there are at least these two differences between the sample and population perspectives: 1. a difference in the emittance and 2. a difference in the time derivatives of the moments. While the statistical kinematics are exact in the sample perspective, they are only exact in the population perspective under the assumption of a collision-less (Vlasov) model or if an exact collision term is available and is included in the kinematics. Furthermore, as demonstrated below, the sample perspective lends itself to some very simple, convincing analyses whose corresponding analyses in the population perspective are intricate. This is not to say the population perspective is in anyway inferior to the sample perspective, just different. For the rest of the paper we focus on the sample perspective and the analysis of the dynamics of second order sample statistics and specifically the emittance dynamics.

III. EXACT SECOND ORDER SAMPLE STATISTICS EVOLUTION

A. General considerations

We return to the definition of the average of a physical parameter, a , across all particles in an ensemble, Eq. (11). In the language of statistics, a is called a random variable and a_i is the value of the random variable for the i^{th} particle within a specific sample.

As classical mechanics is deterministic, a_i can be mapped back to the values of the initial phase coordinates for that particle, $\vec{x}_{0,i}$ and $\vec{p}_{0,i}$. This mapping can be used effectively in the case of laminar flow, however for chaotic systems a mapping of this type for each particle is usually not analytically tractable. Here we focus on near laminar flow. In most particle beams, parameters like time or mass are the same for all particles. Statisticians call parameters that are the same for all particles “scalars”, but we will call such parameters ensemble constants to avoid confusion with the standard meaning of “scalars” in physics. When the maps between the initial phase position and the phase position at some time t are analytically intractable, molecular dynamics can be thought as a means to provide such a map. However, when the flow is near laminar this map can sometimes be constructed analytically without reference to simulation techniques. This can always be achieved in the differential form, which we call the statistical kinematics. Using such maps in Eqs. (13) and (15) allows us to obtain analytic forms for the evolution of the statistics, such as emittance. To carry out this analysis we use the easily proved statistical relation

$$s_{W a + X b, Y c + Z d} = W Y s_{a,c} + W Z s_{a,d} + X Y s_{b,c} + X Z s_{b,d} \quad (29)$$

where the quantities a, b, c, d are random variables (usually position or momentum of a particle) and W, X, Y, Z are ensemble constants (for instance the mass or time).

Notice, that nowhere in this discussion of the evolution of the statistics have we mentioned the underlying phase-space distribution of the particles, just the value of the random variables. This is due to the fact that this description is independent of the phase-space distribution unless the map itself depends on it.

Before we get to concrete examples, we briefly discuss decomposing the momentum within the sample perspective. Specifically, let \bar{p}_{x_i} represent the expected x -momentum at x_i , namely

$$p_i = \bar{p}_{x_i} + \delta_i \quad (30)$$

In other words δ_i is the deviation of the i^{th} x -momentum from the expected value. In this work we will follow the standard practice in accelerator physics, which is to assume that the momentum fluctuation δ_i is independent of x . Our next question is, “What do we use for the expected value of the momentum?” The answer to this question depends on the system, and we focus on systems where there is a linear relation between the average momentum and

the average position. This is the standard convention in experiments where systems with this linear relation can be precisely controlled using electromagnetic lens' and RF cavities. Experimentalists extract this linear relation from their data by choosing the line of best fit for the distribution in x - p_x space. Due to this linear relation, we can write the expectation for the momentum at x_i as,

$$\bar{p}_{x_i} = \bar{p}_x + \frac{s_{x,p_x}}{s_x^2}(x_i - \bar{x}) \quad (31)$$

where the quantity $\frac{s_{x,p_x}}{s_x^2}$ is the slope of the line of best fit of the x - p_x phase space data and \bar{p}_x represents the average x -momentum of the entire ensemble. Under these definitions, we can write the momentum variance as

$$\begin{aligned} s_{p_x}^2 &= \frac{1}{N} \sum_{i=0}^N (p_{x_i} - \bar{p}_x)^2 \\ &= \frac{1}{N} \sum_{i=0}^N \left(\frac{s_{x,p_x}}{s_x^2}(x_i - \bar{x}) + \delta_i \right)^2 \\ &= \frac{s_{x,p_x}^2}{s_x^2} + 2 \frac{s_{x,p_x}}{s_x^2} s_{x,\delta} + s_\delta^2 \end{aligned} \quad (32)$$

As we assume that δ_i is independent of x_i , then $s_{x,\delta} = 0$ and the second term drops out. Now we introduce the important quantity,

$$\eta_x = s_\delta = \sqrt{s_{p_x}^2 - \frac{s_{x,p_x}^2}{s_x^2}} = \frac{mc\varepsilon_{x,p_x}}{s_x} \quad (33)$$

We call η_x the local momentum spread as it has units of momentum and represents the average width of the momentum about the expected position-momentum line. This quantity already, in its squared form, appears in the literature in many works and under different names^{34–36,44}, often with emphasis on the emittance relation (last relation in Eq. (33)). We introduce a second important statistical parameter which also has units of momentum,

$$\mu_x = \frac{s_{x,p_x}}{s_x} \quad (34)$$

Notice that μ_x can be written as $\mu_x = m \frac{ds_x}{dt}$ by Eq. (21)– that is μ_x can be thought of as the momentum involved with the changing of the x -standard deviation of the ensemble. We call μ_x the linear flow momentum as it is the flow that is often attributed to expansion or contraction of an ensemble as calculated using the line of best fit. The local momentum spread may be written in terms of linear flow momentum as;

$$\eta_x^2 = s_{p_x}^2 - \mu_x^2 \quad (35)$$

Finally $\frac{1}{2m}\eta_x^2$ and $\frac{1}{2m}\mu_x^2$ have units of energy and represent the kinetic energy stored in the local momentum spread and in the linear flow momentum; we will call these quantity the linear heat along x and the linear flow energy along x , respectively.

While this discussion so far has been fairly abstract, we demonstrate two concrete cases where the particle trajectories and hence the maps required for the analysis can be analytically calculated: 1. the non-interacting case with no external forces and 2. the 1D, planar-symmetric model. We will show how the above insights can be used to predict both statistics evolution as well as to classify effects that drive emittance growth. We note here that these two cases are not the only two situations that can employ this mapping approach; for instance, this mapping approach can be applied to cases where the interaction of the particles is replaced by some mean-field force that lends itself to calculation and hence the trajectory of each particle can be deduced. A second example is non-interacting particles that are influenced by external fields. As such situations arise in many accelerator physics applications, the statistical approach described here is quite general.

B. Non-interacting, freely-expanding, relativistic particles

Consider non-interacting particles with no force on them. The position and momentum of such a non-interacting particle with energy E are

$$\vec{x} = \vec{x}_0 + \frac{c^2}{E}\vec{p}_0 t \quad (36a)$$

$$\vec{p} = \vec{p}_0 \quad (36b)$$

Notice that if the particle has a non-zero mass, $\frac{c^2}{E} = \frac{1}{\gamma m}$ and the position equation reduces to the standard equation $\vec{x} = \vec{x}_0 + \frac{1}{\gamma m}\vec{p}_0 t$; however, Eqs. (36a) and (36b) also apply to mass-less particles like photons. We consider the statistics in the x -direction as the statistics in the other directions are analogous; Eqs. (36a) and (36b) in the x -direction are

$$x = x_0 + \frac{c^2}{E}p_{0,x}t \quad (37a)$$

$$p_x = p_{0,x} \quad (37b)$$

Notice that x_0 , $p_{0,x}$, and E are random variables whereas c , and t are ensemble constants. Using Eq. (29), we obtain

$$\begin{aligned} s_x^2 &= s_{x_0 + \frac{c^2}{E} p_{0,x} t}^2 \\ &= s_{x_0}^2 + c^4 t^2 s_{\frac{p_{0,x}}{E}}^2 + 2c^2 t s_{x_0, \frac{p_{0,x}}{E}} \end{aligned} \quad (38a)$$

$$\begin{aligned} s_{x,p_x} &= s_{x_0 + \frac{c^2}{E} p_{0,x} t, p_{0,x}} \\ &= s_{x_0, p_{0,x}} + c^2 t s_{p_{0,x}, \frac{p_{0,x}}{E}} \end{aligned} \quad (38b)$$

$$s_{p_x}^2 = s_{p_{0,x}}^2 \quad (38c)$$

From these relations, we find an explicit expression for the emittance evolution:

$$\begin{aligned} \varepsilon_{x,p_x}^2 &= \varepsilon_{x_0, p_{0,x}}^2 + \frac{c^2}{m^2} t^2 \left(s_{p_{0,x}}^2 s_{\frac{p_{0,x}}{E}}^2 - s_{p_{0,x}, \frac{p_{0,x}}{E}}^2 \right) \\ &\quad - \frac{1}{m^2} t \left(s_{p_{0,x}}^2 s_{x_0, \frac{p_{0,x}}{E}} - s_{x_0, p_{0,x}} s_{p_{0,x}, \frac{p_{0,x}}{E}}^2 \right) \end{aligned} \quad (39)$$

In most treatments of ensembles, the energy is assumed to be approximately the same for all particles⁷; that is, E is treated like an ensemble constant instead of a random variable. In this case, the E can be pulled out of the expressions, and the statistics may be written as

$$s_x^2 = s_{x_0}^2 + \frac{c^4 t^2}{E^2} s_{p_{0,x}}^2 + 2 \frac{c^2 t}{E} s_{x_0, p_{0,x}} \quad (40a)$$

$$s_{x,p_x} = s_{x_0, p_{0,x}} + \frac{c^2 t}{E} s_{p_{0,x}}^2 \quad (40b)$$

$$s_{p_x}^2 = s_{p_{0,x}}^2 \quad (40c)$$

Further under this E is an ensemble constant assumption, note that the emittance is conserved, i.e. $\varepsilon_{x,p_x}^2 = \varepsilon_{x_0, p_{0,x}}^2$. With this observation, we can determine when the width of the distribution reaches a minimum by taking the time derivative of Eq. (38a) and setting the derivative to zero and then solving for the time

$$t_{min \ width} = - \frac{E}{c^2} \frac{s_{x_0, p_{0,x}}}{s_{p_{0,x}}^2} \quad (41)$$

Plugging $t_{min \ width}$ into Eq. (38a), we obtain the minimum width of the distribution to be

$$s_x(t_{min \ width}) = \frac{E}{c} \frac{\varepsilon_{x,p_x}}{s_{p_x}} \quad (42)$$

This means that the spatial width of a non-interacting distribution at the focal point is determined by the size of the emittance and the width of the distribution in momentum space. According to Eq. (32), s_{p_x} can be controlled by manipulating $|s_{x,p_x}|$ when s_x and the local momentum spread are held fixed. This is effectively how a thin lens work. Thus, the minimum width of an ensemble is only limited by the ability to adjust $|s_{x,p_x}|$ — and there are no other effects besides controlling when and how small a bunch focusses. This property of the minimum spatial width being set by the emittance when given a specific focussing $|s_{x,p_x}|$ is one of the main reasons that emittance is of interest.

While this formulation is fairly trivial, we have not seen this approach in the literature and it leads to both new results for simple models and a framework for interacting systems. For example, we point out that the spatial-momentum covariance at $t = t_{min \ width}$ is

$$s_{x,p_x}(t_{min \ width}) = 0 \quad (43)$$

for this non-interacting case. It is fairly trivial to show that this covariance is always zero at the minimum width even in the presence of interactions as it is simply a result of the kinematics; which follows from the general expression,

$$\frac{ds_x}{dt} = \frac{s_{x,p_x}}{s_x} \quad (44)$$

As the focal point is an extremum of s_x , it is then obvious that Eq. (43) is true in general.

C. One dimensional models with Coulomb forces

1. General 1D emittance phase-space dynamics

Consider an ensemble of N -particles each with mass m within the 1D, planar model. This model and models equivalent to it have been used extensively to study the spreading dynamics of pancake bunches generated by ultrafast photo-injectors¹⁻³. Here we precisely resolve the emittance dynamics within these models.

Label the positions, velocities, and accelerations of the i^{th} particle in the ensemble by x_i , v_i , and a_i , respectively. Assuming that the particles in the bunch obey laminar flow, a_i is a constant and the trajectory of each particle is described by

$$x_i = x_{i,0} + v_{i,0}t + \frac{1}{2}a_it^2 \quad (45a)$$

$$v_i = v_{i,0} + a_it \quad (45b)$$

where again 0 in the subscript indicates the initial value of the parameter. Notice that Eqs. (45a) and (45b) are again maps between the phase space at time t and the initial phase space, and therefore the approach we used for the non-interacting case can be used here as well. Substituting Eqs. (45a) and (45b) into Eq. (15), we obtain

$$\varepsilon_{x,p_x}^2 = \frac{1}{c^2} |\mathbf{A}(t)| \quad (46)$$

where $|\cdot|$ again represents the determinant of the contained matrix and $\mathbf{A}(t)$ is the 4×4 matrix

$$\mathbf{A}(t) = \begin{pmatrix} 0 & \frac{1}{2}t^2 & -t & 1 \\ \frac{1}{2}t^2 & s_{x_0}^2 & s_{x_0,v_0} & s_{x_0,a} \\ -t & s_{x_0,v_0} & s_{v_0}^2 & s_{v_0,a} \\ 1 & s_{x_0,a} & s_{v_0,a} & s_a^2 \end{pmatrix} \quad (47)$$

We have placed relevant mathematical details of this derivation in Appendix A. We emphasize that the non-time dependent elements in this matrix are determined from the initial conditions and therefore the emittance growth is completely determined by the initial conditions as one would expect for a deterministic system. In Fig. 1, we demonstrate that this equation perfectly agrees with planar symmetric simulations for various parameters that satisfy our assumption of laminar conditions. This perfect agreement is expected as Eq. (46) is an exact description of emittance growth under laminar flow.

All initial conditions in Fig. 1 begin with 0 emittance and we set the initial velocity to be linearly related to the initial position, i.e. $v_{0,i} = \bar{v}_{0,i} + C(x_{0,i} - \bar{x}_{0,i})$. We call the constant C the chirp, and if it is unknown it can be obtained from

$$C = \frac{s_{x,v_x}}{s_x^2} \quad (48)$$

The emittance growth seen in Fig. 1a is then a result of the distribution having a non-linear relation between the expected momentum at a specified position and x . Specifically in non-uniform cases, the x - p_x relation becomes non-linear, and our linear assumption for this relation results in η_x being larger than the deviation from the true non-linear $x - p_x$ behavior. This in turn results in a growth in the emittance. Note that we are using emittance here to describe rms emittance, and that there is a more general understanding of “true” emittance as it relates to Liouville’s theorem in accelerator physics. The effects of non-linearity on the rms emittance, again henceforth called emittance, is trivially calculable

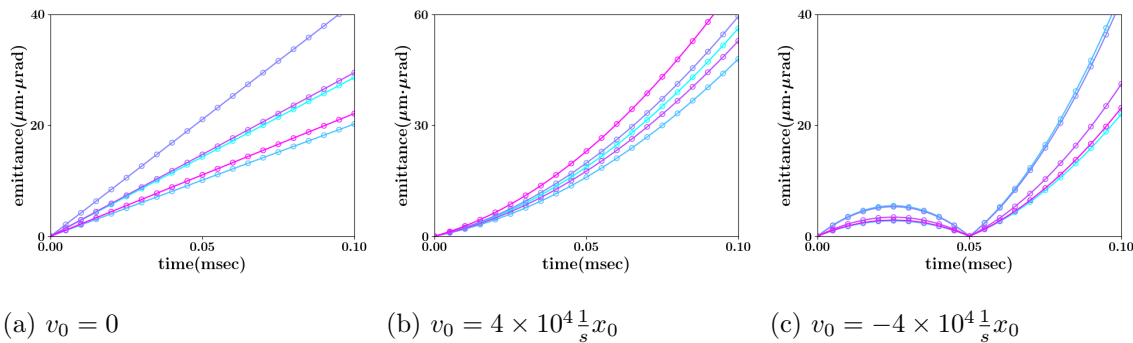


FIG. 1: Graphs of emittance growth under planar symmetry for ensembles of 1,000 planar particles with $\Sigma_{tot} = 1.6 \times 10^{-15} \frac{C}{m^2}$ drawn from the uniform spatial distribution. The initial velocity chirp labels each graph. Different colors represent five different samples of the 1,000 planar particles. Solid lines represent the theoretical prediction based on the initial statistics, as detailed in Eq. (46), and open circles represent simulated results. Notice the exact agreement between the theory and simulation. The curious bump in the last figure is a space-charge effect resulting from the fact that the particles come to rest and reverse their direction at nearly the same time — this bounce-back situation causes the momentum spread to drop precipitously leading to a dramatic decrease in the emittance.

from the initial condition through Eq. (46), and we will calculate the expectation of this effect later in Sections IVC and IVD for Gaussian and quadratic bimodal distributions, respectively. Though we have concentrated on the statistical definition of emittance, it is evident that a deeper analysis of deviations from the non-linear $x - p_x$ relation would yield more insight into the true momentum spread and stochastic energy spread.

The effect of the strength of the self-field within the distribution can also be examined analytically. This can be done by adjusting the charges on the particles in the simulation for the same initial conditions. Specifically, we sampled $10k$ particles from an initially Gaussian distribution. Using the same sample of initial particle placement but varying the assumed charge per each particle allows us to isolate the effect of the self-field. As can be seen in Fig. 2, higher charge densities result in a more rapid emittance evolution. For the special case examined where the initial emittance is 0 and there is no initial velocity, the time constant for this emittance evolution can be shown to be proportional to the square root of the density, i.e. the timescale is essentially the plasma period. Likewise, the slope of the

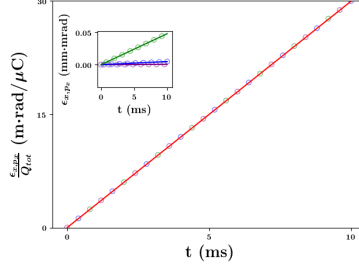


FIG. 2: Plots of emittance growth for the similar ensembles of 10k macro-particles under planar symmetry; solid lines indicate theory and hollow circles indicate simulation. Ensembles were constructed to have all the same statistics except s_{a_x} . Specifically, all ensembles were the same 10k macro-particles sampled from a spatially Gaussian distribution with standard deviation of 1 mm and started from rest. The ensembles differed only by the assumed charges of the macro-particles. This difference corresponds to the distribution with different charge densities which in turn results in different s_{a_x} statistics for the ensembles. Notice that when the charge is small (corresponding to low density), emittance for the simulation does not appreciably increase from its initial value of 0; however, for large charges (corresponding to high density), emittance increases drastically and quickly.

emittance can be shown to be proportional to the square root of the density. Putting these two terms together, for the same period of time the emittance growth will be proportional to the total charge of the distribution as seen in Fig. 2; however, ensembles with more complex initial conditions have an emittance whose dynamics have a more complex dependence on the density.

Of course, we could also consider situations where the initial emittance is non-zero due to say a stochastic factor being included in the initial velocity, i.e. $v_{0,i} = \bar{v}_0 + C(x_{0,i} - \bar{x}_0) + \delta_i$ where δ_i here is a stochastic variable with mean 0 and units of velocity. For the simulations presented here, we chose δ_i from a Gaussian distribution with standard deviation of σ_δ . As can be seen in Fig. 3, for small enough σ_δ , the laminar theory correctly predicts the emittance growth, at least for the time period and parameters examined. However, as expected, the laminar theory begins to diverge from the simulations for moderate σ_δ 's, and for large σ_δ , this divergence is almost immediate. We defer analysis of such “particle cross-over” effects for future studies.

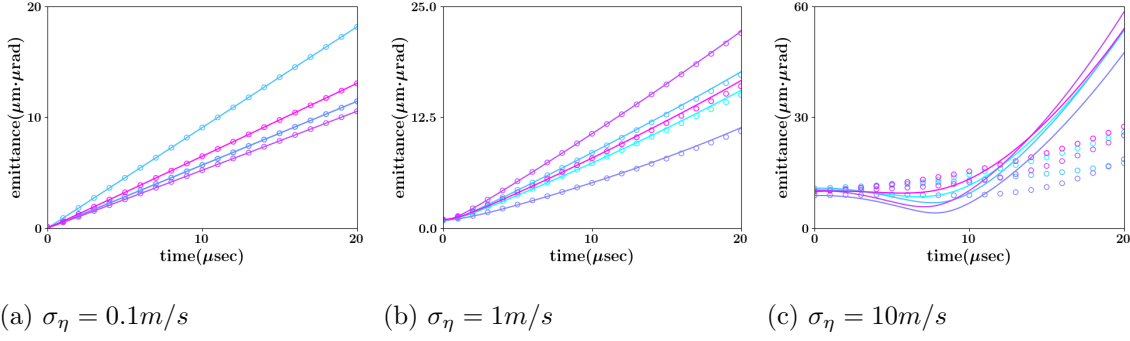


FIG. 3: . The effect of non-laminar flow on the laminar theory of emittance for the evolution of the uniform distribution of 100 planar particles with $\Sigma_{tot} = 1.6 \times 10^{-15} \frac{C}{m^2}$ and the initial width of $1mm$. The parameter σ_δ indicates the standard deviation of the stochastic variable δ_i with mean 0 in the equation $v_{0,i} = \bar{v}_0 + C(x_{0,i} - \bar{x}_0) + \delta_i$. For (a) $\sigma_\eta = 0.1 \frac{m}{s}$ the order of particles remains the same in 4 of the 5 simulations, and all simulations are in agreement with the theory. For (b) $\sigma_\delta = 1 \frac{m}{s}$ particle crossover events that change the order of the particles are seen in all 5 simulations. While the theory is still fairly accurate over the time of the simulation, deviation can be seen later in the simulation. For (c) $\sigma_\delta = 10 \frac{m}{s}$ crossover events are again seen in all 5 simulations; however, the laminar prediction quickly diverges from the simulated results.

IV. STATISTICAL DYNAMICS FROM INITIAL POPULATIONS

A. Expected 1D emittance dynamics of a cold bunch

In the previous section, we obtained an exact expression for the emittance growth that is determined entirely from the initial conditions from the sample perspective. Here we consider the expected emittance growth based on an initial population distribution which is relevant to experiments where the initial population is known, for example at photocathodes. For the sake of simplicity, we assume that all particles start from rest. Thus using Eq. (46) we may write

$$\varepsilon_{x,p}^2 = \frac{s_{x_0}^2 s_a^2 - s_{x_0,a}^2 t^2}{c^2} \quad (49)$$

and the expectation of this is

$$\begin{aligned}\langle \varepsilon_{x,p}^2 \rangle &= \frac{\langle s_{x_0}^2 s_a^2 \rangle - \langle s_{x_0,a}^2 \rangle}{c^2} t^2 \\ &= \frac{1}{c^2} (\sigma_{x_0}^2 \sigma_a^2 - \sigma_{x_0,a}^2 + \text{cov}(s_{x_0}^2, s_a^2) - \text{var}(s_{x_0,a})) t^2\end{aligned}\quad (50)$$

analogous to Eq. (16).

In this section, we assume that the N particles are independently drawn from a 2-dimensional phase density where v_0 is 0 everywhere— we refer to this initial rest state as the initial distribution being cold and it is described by the form,

$$f_{x,p_x,0}(x_0, p_0) = \rho_0(x_0) \delta(p_0) \quad (51)$$

where δ is the Dirac delta function and $\rho_0(x_0)$ is the initial spatial density. Notice that the right hand side of Eq. (50) is determined solely by the initial conditions, so the expected emittance in the non-relativistic 1D model starting from rest can be written as

$$\sqrt{\langle \varepsilon_{x,p}^2 \rangle} = \frac{\sqrt{m_\epsilon^2 + m_{cov}^2}}{c} t \quad (52)$$

where

$$m_\epsilon^2 = \sigma_{x_0}^2 \sigma_a^2 - \sigma_{x_0,a}^2 \quad (53)$$

and

$$m_{cov}^2 = \text{cov}(s_{x_0}^2, s_a^2) - \text{var}(s_{x_0,a}) \quad (54)$$

While m_ϵ^2 is strictly non-negative, m_{cov}^2 is not restricted and can have any value in the real numbers. Further notice that m_ϵ^2 is determined entirely from the population perspective whereas m_{cov}^2 represents statistical fluctuations amongst the sample perspective covariance parameters. In other words, m_{cov}^2 can be thought of as a stochastic contribution to the emittance growth due to finite particle number effects.

In the following cases, we choose our distributions such that either $m_\epsilon = 0$ or $m_\epsilon \gg m_{cov}$. When $m_\epsilon = 0$, Eq. (52) reduces to

$$\sqrt{\langle \varepsilon_{x,p}^2 \rangle} = \frac{|m_{cov}|}{c} t. \quad (55)$$

When $m_\epsilon \gg m_{cov}$, Eq. (52) can be approximated by

$$\sqrt{\langle \varepsilon_{x,p}^2 \rangle} \approx \left(\frac{m_\epsilon}{c} + \frac{m_{cov}^2}{2cm_\epsilon} \right) t \quad (56)$$

As m_{cov}^2 can be thought of as a measure of the stochastic contributions to the emittance growth, define

$$m_{stoch} = \begin{cases} \frac{|m_{cov}|}{c}, & m_\epsilon = 0 \\ \frac{m_{cov}^2}{2cm_\epsilon}, & m_\epsilon \gg m_{cov}^2 \end{cases} \quad (57)$$

so that $\sqrt{\langle \varepsilon_{x,p}^2 \rangle} \approx \left(\frac{m_\epsilon}{c} + m_{stoch} \right) t$ in general.

We now use the initial population distribution to obtain m_ϵ . To obtain this quantity, five expectations need to be calculated from the population distribution: $\langle x_0 \rangle$, $\langle a \rangle$, $\langle x_0^2 \rangle$, $\langle a^2 \rangle$, and $\langle x_0 a \rangle$. In the remainder of this section, we show how to obtain these expectations from an arbitrary population distribution of the form expressed in Eq. (51). In the following sections, we specifically calculate these expectations, and therefore the associated expected emittance, for the uniform, Gaussian, and the quadratic bimodal distributions, and we compare these expectations to simulations.

Consider the 3D charge density $\rho_q(x, y, z; t)$. Assuming planar symmetry, this distribution may be decomposed^{3,38,39}

$$\rho_q(x, y, z; t) = \Sigma_{tot} \rho(x; t) \quad (58)$$

where Σ_{tot} is a constant with units of charge per unit area and $\rho(x; t)$ has units of inverse length and is a probability-like distribution that normalizes to 1. From this distribution, we can calculate the acceleration of a Lagrangian particle with charge q and mass m at x_0 :

$$a = a(x_0) = \frac{q \Sigma_{tot}}{2m\epsilon_0} \left(\int_{-\infty}^{x_0} \rho_0 d\tilde{x} - \int_{x_0}^{\infty} \rho_0 d\tilde{x} \right) \quad (59)$$

For a distribution symmetric about $x_0 = 0$, Eq. (59) reduces to

$$a = \frac{q \Sigma_{tot}}{m\epsilon_0} \int_0^{x_0} \rho_0 d\tilde{x} \quad (60)$$

Notice that regardless of the specifics of the 1D real-space distribution,

$$\langle a \rangle = 0 \quad (61)$$

as required by Newton's third law. Furthermore, notice that the particles are uniformly distributed in acceleration space,

$$\langle a^2 \rangle = \frac{q^2 \Sigma_{tot}^2}{12m^2 \epsilon_0^2} \quad (62)$$

again regardless of the specifics of the 1D real-space distribution — if this somewhat surprising observation is concerning to the reader, we encourage the reader to calculate $\langle a^2 \rangle$ themselves in the cases we discuss shortly. Finally, we treat the population as a continuum and therefore

$$\langle x_0 \rangle = 0 \quad (63)$$

for distributions symmetric about $x_0 = 0$. Thus without reference to the specifics of the population distribution profile, we already know 3 of the 5 required expectations. The remaining 2 expectations, $\langle x_0^2 \rangle$ and $\langle x_0 a \rangle$, are distribution specific.

B. Uniform

For the uniform distribution

$$\rho_0(x_0) = \begin{cases} \frac{1}{L}, & -\frac{L}{2} \leq z_0 \leq \frac{L}{2} \\ 0, & else \end{cases} \quad (64)$$

Using this in Eqs. (60) and (6) we get

$$a(x_0) = \frac{q\Sigma_{tot}}{m\epsilon_0} \frac{x_0}{L} \quad (65a)$$

$$\langle x_0^2 \rangle = \frac{L^2}{12} \quad (65b)$$

$$\langle x_0 a \rangle = \frac{q\Sigma_{tot}L}{12m\epsilon_0} \quad (65c)$$

resulting in Eq. (53) becoming

$$m_e = 0 \quad (65d)$$

Thus, the expected emittance growth from the population theory of the evolution of the uniform distribution is zero as is generally recognized by the community. Thus, the emittance growth will be determined by m_{stoch} solely.

We employed M -shell simulation with $M = 10^4$, $L = 0.1\mu\text{m}$, and $\Sigma_{tot} = 8 \times 10^{-13} \frac{C}{m^2}$ to model the evolution of the uniform distribution. The parameter M is used instead of N to emphasize a point — changes in M are decoupled from changes in the total charge. Often for N -particle simulations, each particle across simulations have the same charge

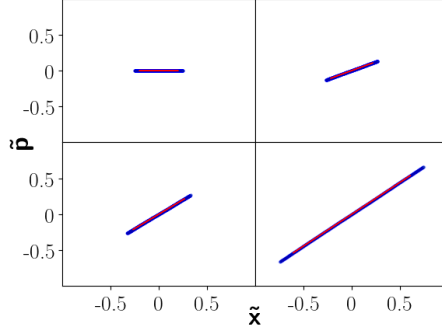


FIG. 4: The normalized ($\tilde{x} = \frac{x}{n_x}$ with $n_x = 0.2 \mu\text{m}$, $\tilde{p} = \frac{p}{n_p}$ with $n_p = 2 \times 10^{-7} mc$) phase-space of a uniform M -shell simulation with $L = 0.1 \mu\text{m}$, $\Sigma_{tot} = 8 \times 10^{-13} \frac{C}{m^2}$, and $M = 10^4$ at 4 distinct times: (top-left) initial, (top-right) 1 ns, (bottom left) 2 ns, (bottom right) 5 ns. Blue circles are the phase-space positions of the 10^4 macro-particles, and the red ellipse, which looks like a line segment directly over the middle portion of the blue circles, corresponds to the rms ellipse associated with the covariance statistics scaled by $2\sqrt{2}$.

resulting in an increase in N indicating an increase in the total charge. Here assign the charge per particle as $\frac{\Sigma_{tot}}{M}$ so that we can independently vary the number of particles and the total charge to more cleanly examine finite particle effects. Fig. 4 shows the phase-space at four distinct times of one such simulation. While the phase-space looks like a straight line, very small variations in the position lead to non-zero emittance; in contrast, the population expectations predict exactly an emittance of zero. This suggests that this emittance growth is entirely stochastic as anticipated by Eq. (55). This non-zero emittance can be seen in Fig. 5 for 3 simulations with different choices of macro-particles but the same total amount of charge. The slope, m_{stoch} , of this non-mean-field theory emittance growth appears to be linear, as expected, and is dependent on the choice of M . For clarity, call the quantity $\sqrt{M}m_{stoch}$ the scaled stochastic slope. The scaled stochastic slope plotted against M across 500 M -shell simulations of the initially uniform distribution with these parameters but for each of 7 choices of M ranging from $1k$ to $100k$ can be seen in Fig. 6. One-way ANOVA³⁷ with $df_1 = 499$ and $df_2 = 3493$ was employed to test the null hypothesis that all scaled slopes were the same, and the associated F-statistic was 0.78, which accepts the null hypothesis when $\alpha \leq 0.05$. This implies that the slope for rms emittance growth in the

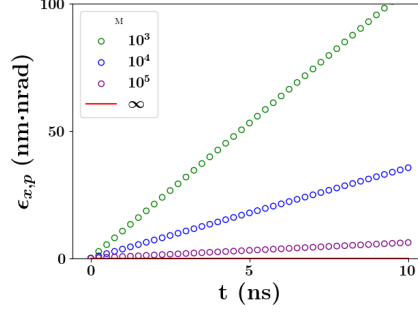


FIG. 5: The emittance growth of an initially uniform distribution starting from rest simulated with M -shell simulations for various values of M (circles) or modeled with mean-field theory (red horizontal line at $y=0$). While theory predicts no emittance growth, stochastics of the M -shell simulations result in apparently linear growth with small slopes that depend on M .

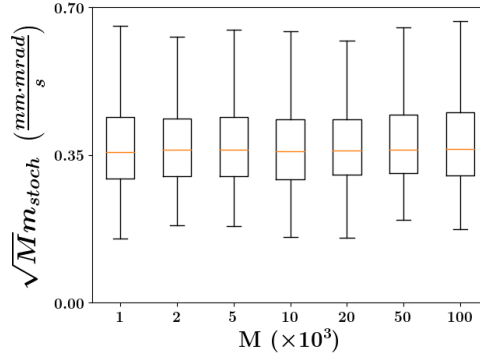


FIG. 6: Box-plots of the scaled stochastic slope for different values of M generated from 3500 uniform M -shell simulations. ANOVA concludes that all simulations have the same scaled slope of $0.38 \pm 0.11 \frac{\text{mm-mrad}}{s}$.

uniform planar symmetric distribution is $m_{stoch} = \frac{0.38 \pm 0.11}{\sqrt{M}} \frac{\text{mm-mrad}}{s}$. This result means that the stochastic and finite-particle effects introduce positive, non-zero emittance growth for systems characterized by a uniform distribution evolution.

C. Gaussian

We now examine the Gaussian 1D distribution with standard deviation σ_{x_0}

$$\rho_0(x_0) = \frac{1}{\sqrt{2\pi}\sigma_{x_0}} e^{-\frac{x_0^2}{2\sigma_{x_0}^2}} \quad (66)$$

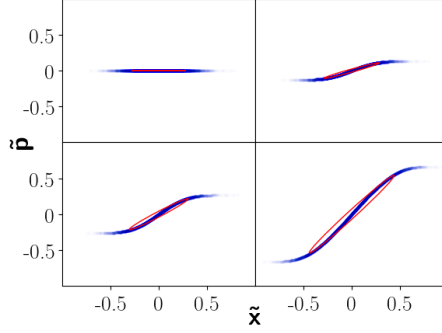


FIG. 7: The normalized ($\tilde{x} = \frac{x}{n_x}$ with $n_x = 0.5 \mu\text{m}$, $\tilde{p} = \frac{p}{n_p}$ with $n_p = 2 \times 10^{-7} mc$) phase-space of a Gaussian M -shell simulation with $\sigma_{x_0} = 0.1 \mu\text{m}$, $\Sigma_{tot} = 8 \times 10^{-13} \frac{C}{m^2}$, and $M = 10^4$ at 4 distinct times: (top-left) initial, (top-right) 1 ns, (bottom left) 2 ns, (bottom right) 5 ns. Blue circles are the phase-space positions of the 10^4 macro-particles, and the red ellipse corresponds to the the rms ellipse associated with the covariance statistics scaled by $2\sqrt{2}$.

Using this in Eqs. (60) and (6) we get

$$a(x_0) = \frac{q\Sigma_{tot}}{2m\epsilon_0} \text{erf}\left(\frac{x_0}{\sqrt{2}\sigma_{x_0}}\right) \quad (67a)$$

$$\langle x_0^2 \rangle = \sigma_{x_0}^2 \quad (67b)$$

$$\langle x_0 a \rangle = \frac{q\Sigma_{tot}\sigma_{x_0}}{2m\sqrt{\pi}\epsilon_0} \quad (67c)$$

resulting in Eq. (53) becoming

$$\begin{aligned} m_\epsilon &= \sqrt{\frac{1}{12} - \frac{1}{4\pi} \frac{q\Sigma_{tot}\sigma_{x_0}}{m\epsilon_0}} \\ &\approx 0.0613 \frac{q\Sigma_{tot}\sigma_{x_0}}{m\epsilon_0} \end{aligned} \quad (67d)$$

We again employed M -shell simulation with $M = 10^4$, $\sigma_{x_0} = 0.1\mu\text{m}$, and $\Sigma_{tot} = 8 \times 10^{-13} \frac{C}{m^2}$ to model the evolution of Gaussian distribution. Unlike the uniform distribution, Fig. 7 shows that visible non-linearity arises during the simulation. Simulations with 3 different M with the same total charge agree well with theory as can be seen in Fig. 8 allowing us to make the assumption that $m_\epsilon^2 \gg m_{cov}^2$.

As expected, small variations of the slope are also evident in Fig. 8. To explore this variation, we subtracted the $\frac{m_\epsilon}{c}t$ from the emittance leaving us with m_{stoch} . Again, we examine the scaled stochastic slope, $\sqrt{M}m_{stoch}$. The scaled stochastic slope plotted against

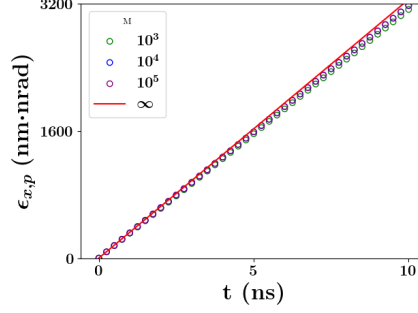


FIG. 8: The emittance growth of an initially Gaussian distribution starting from rest simulated with M -shell simulations for various values of M (circles) or modeled with mean-field theory (red line). All simulations are fairly similar to theory suggesting the non-linearity captured by the mean-field model dominates stochastic effects for the Gaussian distribution.

M across 500 M -shell, same total charge simulations of the initially Gaussian distribution with these parameters but for each of 7 choices of M ranging from $1k$ to $100k$ can be seen in Fig. 9. One-way ANOVA with $df_1 = 499$ and $df_2 = 3493$ was employed to test the null hypothesis that all scaled slopes were the same, and the associated F-statistic was 1.95, which still accepts the null hypothesis when $\alpha \leq 0.05$. This implies that the stochastic contribution to the slope for emittance growth in the Gaussian planar symmetric distribution is $m_{stoch} = \frac{0 \pm 0.8}{\sqrt{M}} \frac{mm \cdot mrad}{s}$. For comparison, the mean-field slope is $0.33 \frac{mm \cdot mrad}{s}$ with these parameters which does have the property $m_\epsilon \gg m_{stoch}$ for $M \geq 1000$ as expected; that is the non-linear mean-field effects dominate emittance growth of systems characterized by the Gaussian distribution for sufficient $M > 1000$.

D. Quadratic Bimodal

For the quadratic bimodal distribution

$$\rho_0(x_0) = \begin{cases} \frac{12}{L^3} x_0^2, & -\frac{L}{2} \leq x_0 \leq \frac{L}{2} \\ 0, & else \end{cases} \quad (68)$$

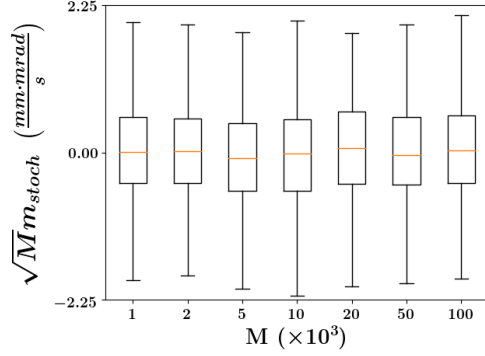


FIG. 9: Box-plots of the scaled stochastic slope for different values of M generated from 3500 Gaussian M -shell simulations. ANOVA concludes that all simulations have the same scaled remainder slope of $0 \pm 0.8 \frac{\text{mm.mrad}}{s}$.

Using this in Eqs. (60) and (6) we get

$$a_s(x_0) = \frac{4q\Sigma_{tot} x_0^3}{m\epsilon_0 L^3} \quad (69a)$$

$$\langle x_0^2 \rangle = \frac{3L^2}{20} \quad (69b)$$

$$\langle x_0 a \rangle = \frac{3q\Sigma_{tot} L}{28m\epsilon_0} \quad (69c)$$

resulting in Eq. (53) becoming

$$\begin{aligned} m_\epsilon &= \sqrt{\frac{1}{12} - \frac{15}{196} \frac{q\Sigma_{tot}\sigma_{x_0}}{m\epsilon_0}} \\ &\approx 0.0825 \frac{q\Sigma_{tot}\sigma_{x_0}}{m\epsilon_0} \end{aligned} \quad (69d)$$

We employed M -shell simulation with $M = 10^4$, $L = 0.1\mu\text{m}$, and $\Sigma_{tot} = 8 \times 10^{-13} \frac{C}{m^2}$ to model the evolution of the bimodal distribution. Fig. 10 shows the phase-space at four distinct times of one such simulation, and this phase distribution has a visible non-linear kink about the origin, although in the opposite direction to the kink seen in the Gaussian distribution, that is related to the non-zero emittance growth of systems described by this distribution. Simulations with 3 different M with the same total charge agree well with theory as can be seen in Fig. 11 again suggesting that we make the assumption $m_\epsilon^2 \gg m_{cov}^2$.

We again subtracted $\frac{m_\epsilon}{c}t$ from the emittance leaving us with m_{stoch} , and we examined the scaled stochastic slope, $\sqrt{M}m_{stoch}$. The scaled stochastic slope plotted against M across 500 N -shell, same total charge simulations of the initially bimodal distribution with these parameters but for each of 7 choices of M ranging from $1k$ to $100k$ can be seen in Fig. 12. One-way

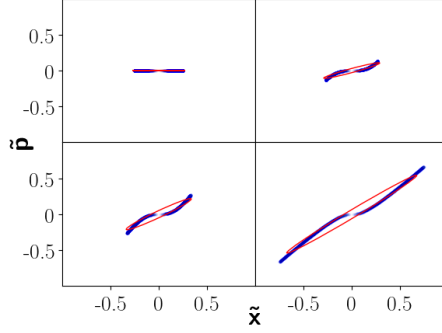


FIG. 10: The normalized ($\tilde{x} = \frac{x}{n_x}$ with $n_x = 0.2 \mu\text{m}$, $\tilde{p} = \frac{p}{n_p}$ with $n_p = 2 \times 10^{-7} mc$) phase-space of a bimodal M -shell simulation with $L = 0.1 \mu\text{m}$, $\Sigma_{tot} = 8 \times 10^{-13} \frac{C}{m^2}$, and $M = 10^4$ at 4 distinct times: (top-left) initial, (top-right) 1 ns, (bottom left) 2 ns, (bottom right) 5 ns. Blue circles are the phase-space positions of the 10^4 macro-particles, and the red ellipse corresponds to the the rms ellipse associated with the covariance statistics scaled by $2\sqrt{2}$.

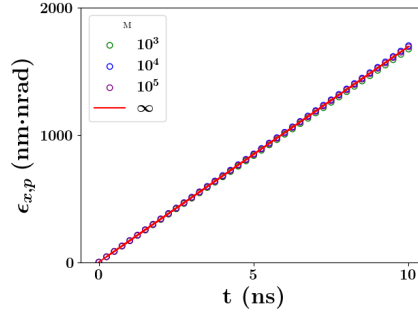


FIG. 11: The emittance growth of an initially bimodal distribution starting from rest simulated with M -shell simulations for various values of M (circles) or modeled with mean-field theory (red line). All simulations are fairly similar to theory suggesting the non-linearity captured by the mean-field model dominates stochastic effects for the bimodal distribution.

ANOVA with $df_1 = 499$ and $df_2 = 3493$ was employed to test the null hypothesis that all scaled slopes were the same, and the associated F-statistic was 0.83, which accepts the null hypothesis when $\alpha \leq 0.05$. This implies that the stochastic contribution to the slope for emittance growth in the bimodal planar symmetric distribution is $m_{stoch} = \frac{0.01 \pm 0.15 \text{ mm}\cdot\text{mrad}}{\sqrt{M} s}$, which is again much smaller than $m_\epsilon = 0.17 \frac{\text{mm}\cdot\text{mrad}}{s}$ for sufficient M . Notice that the dis-

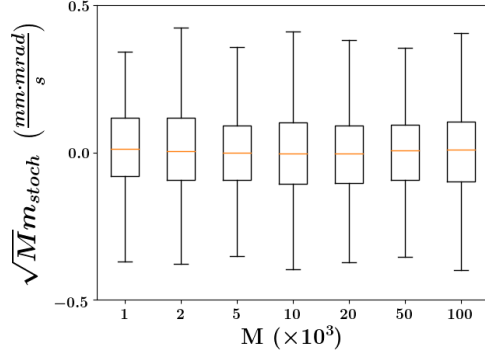


FIG. 12: Box-plots of the scaled stochastic slope for different values of M generated from 3500 uniform M -shell simulations. ANOVA concludes that all simulations have the same scaled slope of $0.38 \pm 0.11 \frac{\text{mm}\cdot\text{mrad}}{\text{s}}$.

tribution of stochastic slopes is again roughly symmetric about zero similar to the Gaussian case but with a smaller standard deviation.

V. THE SAMPLE PERSPECTIVE AND KINETIC ENERGY

Kinetic energy plays a central role in the sample perspective as kinetic energy can be decomposed using ensemble statistics. Namely,

$$\begin{aligned}
 KE &= \sum_{i=1}^N \sum_{j \in \{x,y,z\}} \frac{p_j^2}{2m} \\
 &= \sum_{j \in \{x,y,z\}} KE_j
 \end{aligned} \tag{70}$$

where $KE_j = \frac{p_j^2}{2m}$ is the portion of the kinetic energy contained in the j^{th} dimension. For the planar model, only the kinetic energy of one of these dimensions is relevant. Specifically, the portion of the kinetic energy along x can be written as

$$\begin{aligned}
 KE_x &= \sum_{i=1}^N \frac{p_x^2}{2m} - N \frac{\bar{p}_x^2}{2m} + N \frac{\bar{p}_x^2}{2m} \\
 &= \sum_{i=1}^N \frac{(p_x - \bar{p}_x)^2}{2m} + N KE_{CoM,x} \\
 &= N \frac{s_{p_x}^2}{2m} + N KE_{CoM,x}
 \end{aligned} \tag{71}$$

where $KE_{CoM,x} = \frac{\bar{p}_x^2}{2m}$ is the kinetic energy of a single particle traveling with the mean momentum of the distribution, i.e. the center of mass (CoM) motion of the ensemble. Notice this equality is exact in the sample perspective, and any discussion of energy, so central to physics, thus necessitates an understanding of the momentum variance.

This energy can be further decomposed using the standard notation of emittance. Specifically, using $\mu_x = \frac{s_{x,p_x}}{s_x}$ and $\eta_x^2 = s_{p_x}^2 - \mu_x^2$, the kinetic energy can be written as

$$KE_x = N \frac{\eta_x^2}{2m} + N \frac{\mu_x^2}{2m} + N KE_{CoM,x} \quad (72)$$

While this may not look as if the statistical definition of emittance is used here, remember that emittance is $\varepsilon_{x,p_x} = \frac{1}{mc} s_x \eta_x$. Therefore, if we analyze the physical processes affecting the energy term, $N \frac{\eta_x^2}{2m}$, we can develop a deeper understanding of emittance dynamics. Specifically, $N \frac{\mu_x^2}{2m}$ can be thought of as a mode that contains the kinetic energy of the linear flow motion of the distribution and $N \frac{\eta_x^2}{2m}$ can be thought of as the mode that contains the kinetic energy remaining when the linear flow energy is removed, i.e. the kinetic energy fluctuations or "heat".

One caveat, though, is that $N \frac{\mu_x^2}{2m}$ is an estimate of the flow energy using the linear $x - p_x$ relation that is assumed in almost all of beam physics, and this approximation is sometimes questionable. Fortunately for the planar model we can exactly calculate the kinetic energy of the distribution. Quite remarkably, the kinetic energy of a planar distribution at time t starting from rest at time 0 is given by Eq. (71):

$$KE = \frac{Nm}{2} s_a^2 t^2 \quad (73)$$

where $s_a^2 = \frac{q^2 \Sigma_{tot}^2}{12m^2 \epsilon_0^2}$ by Eq. (61) and Eq. (62). This result is exact regardless of the initial density profile of the distribution. The universality of this result is peculiar to the 1-D constant acceleration case which enable analytic insight that is hard to extract in more complex systems. A calculation of the linear flow energy yields,

$$N \frac{\mu_x^2}{2m} = \frac{Nm}{2} \frac{s_{x_0,a}^2 + s_{x_0,a} s_a^2 t^2 + \frac{1}{4} s_a^4 t^4}{s_{x_0}^2 + s_{x_0,a} t^2 + \frac{1}{4} s_a^2 t^4} t^2 \quad (74)$$

Notice that this estimate is profile specific. Namely, $s_{x_0,a}$ and $s_{x_0}^2$ differ depending on the profile. We have already calculated the expectation of these covariances under the uniform, Gaussian and bimodal distributions in Sections IV B, IV C, and IV D, respectively, so no additional calculation is necessary. For the uniform case, notice we have $s_{x_0,a} = s_{x_0} s_a$.

Putting this into Eq. (74), the uniform case linear expansion energy reduces to Eq. (73); that is, the linear flow energy exactly captures the kinetic energy evolution of the uniform distribution, so when the distribution expands, no energy is transferred to the heating mode. Furthermore, for long time, the linear flow energy of the non-uniform distributions asymptote to Eq. (73); however, for the non-uniform distributions at any real time, $N \frac{\mu_x^2}{2m} < KE$. That is, even though these distributions have the same energy in the expansion mode as the uniform distribution, the statistics we use underestimates the amount of kinetic energy associated with expansion.

Since the heat is the left over energy, any underestimation of the linear flow energy means that a portion of the heat, $N \frac{\eta_x^2}{2m} = N \frac{p_x^2 - \mu_x^2}{2m}$, is actually linear flow energy. In fact, we can easily obtain a functional form for the heat when the planar distribution starts from rest with

$$\begin{aligned} \frac{N}{2m} \eta_x^2 &= \frac{Nm}{2} \frac{c^2 \varepsilon_{x,p_x}^2}{s_x^2} \\ &= \frac{Nm}{2} \frac{s_{x_0}^2 s_a^2 - s_{x_0,a}^2}{s_{x_0}^2 + s_{x_0,a}^2 t^2 + \frac{1}{4} s_a^2 t^4} c^2 t^2 \end{aligned} \quad (75)$$

Of course, this is simply the complementary energy to the linear flow energy in Eq. (74) as their sum gives Eq. (73) in all cases. The evolution of $\frac{N}{2m} \eta_x^2$ of $10k$ planar particles initially with Gaussian-spatial distribution with density $\Sigma_{tot} = 8 \times 10^{-13} \frac{C}{m^2}$ can be seen in Fig. 13. All initially cold-1D distributions exhibit this characteristic, single-hump evolution. This release of heat from the 1D model is qualitatively the same as seen by Maxson et. al in their study of disorder induced heat⁴⁴ in fully 3D systems; however, additional concerns are present in the full 3D model, and we will discuss these concerns shortly.

However, before we move onto the discussion of additional 3D effects, we first further discuss the evolution of the three modes we recognize in our model: the potential energy (U), the linear flow mode, and the linear heat mode. Taking the time derivative of the linear flow energy, we obtain

$$\begin{aligned} \frac{d}{dt} \frac{N}{2m} \mu_x^2 &= \frac{N}{m} \mu_x \dot{\mu}_x \\ &= \frac{N}{m} (\mu_x f_x + \mu_x \theta_x) \end{aligned} \quad (76)$$

where $f_x = \frac{s_{x,F_x}}{s_x}$ can be thought of as the self-force at one standard deviation within the spatial-force distribution as expected from linear regression in the same way $\mu_x = \frac{s_{x,p_x}}{s_x}$ is the

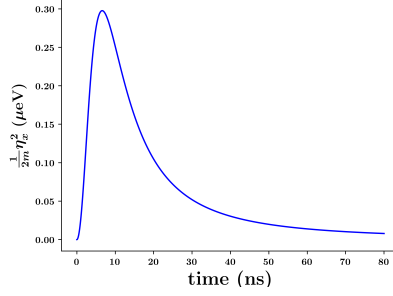


FIG. 13: The evolution of the linear heat along x , $\frac{1}{2m}\eta_x^2$, for an ensemble of $10k$ planar particles initially with Gaussian-spatial distribution with density $\Sigma_{tot} = 8 \times 10^{-13} \frac{C}{m^2}$ and initial width of $0.1 \mu m$. Notice that kinetic energy is initially released as heat into the distribution, and then this heat is rapidly lost to expansion. This is qualitatively similar to the evolution of the Mean Transverse Energy (mathematically identical what we are calling the linear heat along x) seen by Maxson et. al⁴⁴. We note that Maxson et al.’s explanation for this effect is a phenomenological $3D$ model that captures the phenomenon with fitted parameters while we present an analytic $1D$ model that does not yet quantitatively capture the effect described by Maxson et. al.

corresponding momentum, and $\theta_x = \frac{1}{m} \frac{\eta_x^2}{s_x}$ can be thought as some kind of effective heating force. Taking the time derivative of the heat we obtain

$$\begin{aligned} \frac{d}{dt} \frac{N}{2m} \eta_x^2 &= \frac{N}{2m} \frac{d}{dt} (s_{p_x, p_x} - \mu_x^2) \\ &= \frac{N}{m} (s_{p_x} \phi_x - \mu_x f_x - \mu_x \theta_x) \end{aligned} \quad (77)$$

where $\phi_x = \frac{s_{p_x, F_x}}{s_{p_x}}$ is analogous to f_x and μ_x except for it is the linear prediction of the momentum-force relation. Notice that these equations are simply two of the three statistical kinematics equations used to derive the envelope equations. Inspection of these terms allows us to isolate the three “power channels” through which energy is transferred between these modes and the potential energy as can be seen in Fig. 14.

If we consider a non-interacting model, there is no force. In such a model, $f_x = 0$ and $\phi_x = 0$ by definition. The term θ_x is only zero if the bunch has no heat (and hence zero emittance), otherwise it is not zero. So for any non-interacting model with non-zero emittance, there is energy flow between the linear heat and the linear flow energy, given by $\frac{N}{2m} \mu_x \theta_x$, as the bunch evolves. This is the only power channel available to the non-interacting

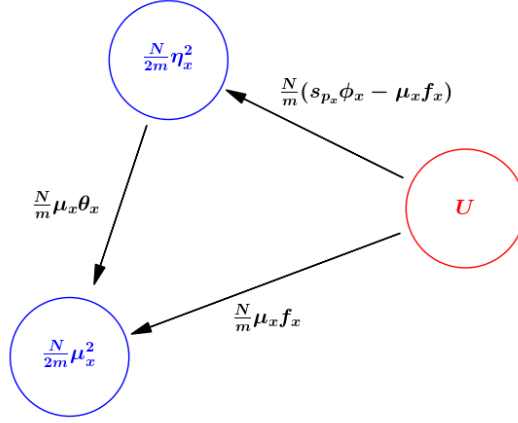


FIG. 14: Exact schematic of the non-relativistic kinetic energy and potential energy of a generic 1D system from the sample perspective. The labelled circles represent modes where energy can be found, and the arrows represent power channels across which energy can be exchanged between the modes. Note that the label on the power channel may be negative thus reversing the direction of energy flow. U represents potential energy,

$$\eta_x = \sqrt{s_{p_x}^2 - \mu_x^2}, \quad f_x = \frac{s_{x,F_x}}{s_x}, \quad \phi_x = \frac{s_{p_x,F_x}}{s_{p_x}}, \quad \text{and} \quad \theta_x = \frac{1}{m} \frac{\eta_x^2}{s_x}.$$

model, and we will call this channel the non-interacting channel.

When we consider interacting models, we note that the power channel labelled by $\frac{N}{m}(s_{p_x}\theta_x - \mu_x f_x)$ can also be written as $\frac{N}{2}mc^2 \frac{1}{s_x^2} \frac{d\varepsilon_{x,p_x}^2}{dt}$ — that is, this energy flows across this power channel only if emittance changes. We will call this channel the emittance change channel. Therefore, the envelope equations, which conserve emittance, do not have any energy exchange directly between the potential and the heat through the emittance change channel. Instead, they have the non-interacting channel and the additional power channel between the potential and the linear flow energy, which we will call the flow channel. Of course, if we were to use a model that does not conserve emittance, all three channels; non-interacting, flow, and emittance change, would be accessible — this is the case we see in the planar model.

We can now qualitatively describe what is happening in Fig. 13. When the planar distribution starts from rest, the potential is converted to linear flow energy and linear heat through the flow and emittance change channels, respectively. Again, the emittance change channel occurs due to deviations from linearity. However, as the distribution begins to expand and heat up, μ_x and the heat both get larger. Eventually, these two values

are sufficient to result in the non-interacting channel, $\frac{N}{2m}\mu_x\theta_x$, becoming larger than the emittance change channel resulting in a depletion of the linear heat to linear flow energy despite the fact that the emittance channel remains non-zero.

So this brings us back to why Fig. 13 is so similar to the plot of disorder induced heating seen at least by Maxson et. al.⁴⁴. The reason is because the schematic in Fig. 14 is still correct in $3D$ with a couple of modifications. First, instead of just KE_x , we now have KE_y and KE_z , which can be split up similarly. The only way to transfer energy between the dimensions is through the potential. A full schematic of this picture is seen in Fig. 15. Secondly, as the force in $3D$ is proportional to $\frac{1}{r^2}$, displacements from the reference distribution, which is no longer uniform except in the continuous case, will affect the potential. We will examine this potential difference both from stochastic effects and from the global profile in future work, but we point out that the release of this additional potential is analogous to the non-linear effects already seen in $1D$. Finally, in the planar model, the kinetic energy of the bunch increases toward infinity whereas the $3D$ dynamics quickly deplete the potential energy. So while the $1D$ effects will not capture this additional disorder induced heating, they do evolve similarly.

VI. DISCUSSION

Here we have presented an approach to non-equilibrium beam dynamics we are calling the sample perspective. By changing the focus of analysis from the expectation operator dependent on the population density to the mean operation on a specific sample, we are able to obtain exact equations for the time evolution of the sample statistics. The theoretical advantage of the sample perspective is that it yields new analytic approaches, useful and complementary physical insight, and it may lead to a systematic calculation of all moments though here we focus on the second moment. Moreover, for well behaved distributions, knowledge of all moments provides an effective analysis of non-equilibrium distributions, provided they are well behaved. More standard non-equilibrium dynamic approaches, like Vlasov's equation or the BKG hierarchy of equations can be computationally difficult and require different and complementary analytic approaches. As seen here, the sample perspective supplies surprisingly simple exact descriptions for the case of laminar flows in one dimension, and a number of additional results including results for higher dimensional

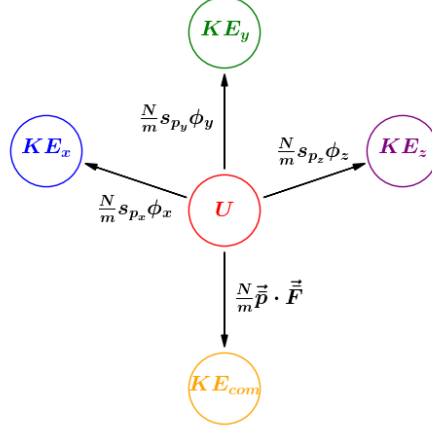


FIG. 15: Exact schematic of the non-relativistic kinetic energy and potential energy of a generic 3D system from the sample perspective. The labelled circles represent modes where energy can be found, and the arrows represent power channels across which energy can be exchanged between the modes. Note that the label on the power channel may be negative thus reversing the direction of energy flow. U represents potential energy, $KE_{com} = N \sum_{j \in \{x,y,z\}} \frac{\bar{p}_j^2}{2m}$ is the kinetic energy of the center of mass, and $KE_j = \frac{s_{p_j}^2}{2m}$ for $j \in \{x, y, z\}$. Notice that the center of mass mode could be split up into three modes, x , y , and z , but we have not done so here to simplify the schematic as we are not concerned with center of mass motion in this manuscript. Further notice that all inter-dimensional energy transfer needs to pass through the potential — i.e. there needs to be an interaction between particles where the energy can be stored. Finally, KE_j can be split up as in Fig. 14 for each j .

models are being developed.

Returning to the difference between the population and sample perspectives, we point out the collisions present in the population perspective are absent from the sample perspective. Collisions are required to fully capture the interactions in the population theory, but the interactions are exactly captured through the interparticle forces in the sample paradigm. Nevertheless there are many ways in which the collisions required in the population perspective can be estimate by using the sample calculations, for example calculations of the variance of the emittance in the sample perspective may be used to estimate the collision term in the population perspective, as will be described elsewhere. It is important to distinguish between the collision term in the population perspective and scattering events which

are exactly captured in the sample perspective, provided the exact force is used. Moreover in a classical calculation, and assuming a system that is not chaotic, the emittance dynamics is deterministic provided the initial conditions are known exactly, as noted by Sacherer¹³.

Of course, collision-less is not synonymous with emittance conserving; specifically, we saw emittance growth in our planar symmetric model. Easy to appreciate are the global non-linearities that arise in phase space that are due to non-linearities that arise from real-space planar distribution being non-linear. Anderson calculated the effect of such non-linearities using the population perspective well over 3 decades ago¹⁸, and the community is quite aware of their role⁸. Of course, we saw, especially in the analysis of uniform planar-symmetric distributions, that stochastic effects can also play a significant role; however, stochastic effects, as presented in the planar symmetric model, are in fact just another form of non-linearity. It is common to think of the force in terms of the mean field force, but finite particle effects, even in the planar symmetric model, result in deviations from the expected variances and covariances. In turn, these deviations introduce additional non-linear effects. In the case of the mean-field uniform distribution, the introduced non-linearities are dominant as the mean-field non-linearities are completely absent. In the case of the Gaussian and quadratic bimodal distribution examined in this work, the additional non-linearities are much smaller than the mean-field non-linear contributions. Furthermore, these stochastic non-linearities may in fact make such non-uniform distributions more-linear. So it should come as no surprise that the average uniform emittance slope increase due to stochastic effects is non-zero but the analogous term for the non-uniform cases is symmetric about zero. In fact, these stochastic non-linearities can be obtained analytically, but such analysis is involved and beyond the scope of this introductory presentation. We will present such theory in future work.

Again, the use of the covariance statistics is inherently linear as $\frac{s_{x,p_x}}{s_x^2}$ is the slope of the line of best fit relating x and p_x . So the (statistical) emittance growth can be argued to be an artifact of the linear statistics used to define the second moments. This is an important feature of the emittance utilized in the field of accelerator physics, and is due to the fact that linear optics are generally used when manipulating charged particle beams, and therefore, this linear statistic is appropriate for such standard techniques. Our second counter argument is theoretical. The most natural nonlinear choice for the function relating the position and momentum at t would be to choose the average momentum at a specific

position. Doing so eliminates the mean-field portion of the slope, m_{mean} , from Eq. (54). That is, under this alteration of the statistics, the expected emittance growth would follow m_{stoch} , which represents how the sample distribution differs from the population distribution, solely. As we can largely separate out m_{stoch} from the underlying distribution, such non-linear treatment does not provide any additional physical insight. Of course, we could adopt the strategy to remove the non-linearities in the measure by finely-slicing and measuring the emittance of each slice as an alternative method of getting rid of the non-linearities. However, again this reduces to calculating m_{stoch} . Therefore, we conclude that the effects on emittance of these non-linearities should be separated out in future theoretical treatments, and a better understanding of m_{stoch} is needed.

We close this section by emphasizing again that the sample perspective is exact if the interparticle force and initial statistical configuration are exactly known; specifically, the full 3D statistical kinematic equations, a generalization of Eqs. (19a) - (19c), exactly describes the evolution of the statistics as alluded to by Sacherer. Central in such analyses is the force, and the force is where the sample and population perspectives are most divergent. Specifically, in the sample perspective the force on each particle is exactly specified by the N values of the particles in phase space; in the population perspective, the force is ill-defined although often approximated by the mean field force¹³. The role of the force can be easily seen in the two cases we examined here. Namely, the force is trivially calculated from the ensemble as it is either exactly 0 (in the non-interacting case) or is trivially constant for each particle (the laminar planar symmetric case). This exact specification of the force is why these situations lead to exact solutions to the evolutions of the statistics. On the other hand in full 3D dynamics, the force is much more complicated and instead needs to be approximated, and one such approximation, the mean-field force approximation, to close the system of equations is already in the literature¹³ and in Eq. (23). Moreover our previous work on the forces present in laminar flow Coulomb explosion problems^{3,38,39} can be straightforwardly extended to the forces in the sample perspective for particle configurations exhibiting laminar flow.

VII. CONCLUSION

In this work, we have formalized the sample perspective and compared it to the population perspective utilized extensively in the literature. We showed that these perspectives give fundamentally different statistical results in at least two cases: 1.) the estimation of the emittance and 2.) the determination of derivatives. As well as providing new approaches to analysis, the sample perspective provides important new physical insights, and is complementary to the insights gained from the population perspective. A key distinction between the sample and population perspectives is that the including of collisions is critical to an exact analysis within the population perspective, but the sample perspective provides an exact description from knowledge of the interparticle forces alone. In this work we concentrated on the sample perspective, however a combined analysis utilizing both the population and sample perspectives is a profitable direction for future work.

In this work we used the sample perspective to provide an exceptionally succinct and general analysis of the evolution of the ensemble statistics of non-interacting particles. We showed how emittance arises in the non-interacting theory as a constraint on the waist of the distribution when focussed. Specifically, we showed how emittance is conserved in such non-interacting models under the assumption that all particles have the same Lorentz factor, i.e. the same energy, but we point out that emittance changes when the ensemble has a non-zero energy spread as can be calculated by Eq. (39). In practice where the energy spread is small, the resulting emittance change during experimentally relevant times is usually much smaller than the inherent emittance of the ensemble. This is why non-interacting bunches are often treated as conserved emittance systems^{7,13}; however, this is not strictly true as can again be seen in Eq. (39).

Utilizing planar models used extensively in the UEM community to describe the spreading of pancake bunches, we calculated exactly the emittance dynamics for these models, which is an important theoretical result. We showed that the emittance dynamics in the planar model are purely a consequence of global and stochastic non-linearities, and that the global non-linearities may be obtained from the *a priori* distribution using mean-field theoretical techniques. While emittance growth due to non-linearities is well appreciated by the community⁸, we specifically calculated the emittance growth equations for the cold planar symmetric uniform, Gaussian, and quartic bimodal distributions. We explained how

these equations may provide insight into disorder induced heating, and we emphasized that the stochastic portion of emittance evolution warrants further attention.

The analysis for the cold distributions is easily extended to cases that do not start from rest by including a non-zero velocity in Eq. (A1), for example an initial chirp. Of course, additional expectations are necessary, but the predictions should be similarly accurate. In such a case, additional powers of time become important resulting in the emittance becoming non-linear as seen in Fig. 1, but the coefficients in front of the powers of time can be calculated if the initial distribution in position and velocity space is assumed. In fact, the reason we examine the coefficient in front of the squared time is that the case examined here has only a delta function in velocity space which results in all coefficients except the projection to position-acceleration space being zero.

While this formulation requires that the initial conditions are known, we point out that in Fig. 1 that drawing the particles from the same initial distribution results in solutions that can also be thought of as an evolving distribution; that is an N -particle ensemble is simply a single sample point in $6ND$ -phase-space and we are concerned with the evolution of the spread of a statistic from repeated samples from that space. This is the perspective we used to calculate the mean emittance growth for our three planar symmetric distributions. In fact, we can describe higher order moments of this distribution using this approach; however, such a description is statistically intricate.

An important computational result present here is the spread in the emittance due to finite particle number, which we find scales as $\frac{1}{\sqrt{M}}$, where M is the number of macro-particles chosen in the simulation. Specifically, this portion of the slope for the uniform distributions was found to be $\frac{0.38 \pm 0.11}{\sqrt{M}} \frac{\text{mm} \cdot \text{mrad}}{\text{s}}$ as can be seen in Fig. 6. On the other hand, both the initially Gaussian and quadratic bimodal distributions were found to be distributed about $0 \pm \text{some value over } \sqrt{M}$ instead as seen in Figs. 9 and 12. These $\frac{1}{\sqrt{M}}$ scalings suggests a statistical origin. As Eq. (53) describes the emittance growth of non-relativistic, cold distributions, it is apparent that this variation in slope is due to stochastic factors in the initial position-acceleration space obtained from sampling the underlying $6ND$ population distribution. Specifically, the estimates we obtained for $\epsilon_{x,p}$ from mean-field theory lack these stochastic factors which should provide “error bars” on our predictions. Of course, as the mean-field volume for the uniform real-space distribution is zero, any stochastic fluctuation should increase this volume resulting in the expectation that the fluctuations introduce a

solely positive slope component consistent with $0.38 \frac{mm \cdot mrad}{s}$. On the other hand, both the Gaussian and bimodal distribution have significant initial volume, so it is no surprise that (a.) this volume dominates the stochastic factor and (b.) stochastic factors appear to be equally likely to drive this volume either up or down consistent with the expectation of $0 \frac{mm \cdot mrad}{s}$ we observed for these cases.

Notice, though, that the $\frac{1}{\sqrt{M}}$ scaling was determined from computations, and a more complete statistical model should have additional coupling terms between the stochastic effects and the geometric details. Specifically, one would expect that a distribution closer to the uniform distribution should have a finite stochastic contribution between 0 and $0.38 \frac{mm \cdot mrad}{s}$. In fact, we examined the emittance growth of the initially semi-circular distribution, not presented, and observed evidence of this behavior, but the means of the scaled remainder slope, m_{stoch} , for differing values of M were not the same until $M > 10,000$ suggesting a more complex general form for the deviation in slope other than $\frac{1}{\sqrt{N}}$, particularly at small N .

We also presented how the covariance statistics relate to kinetic energy, and showed how the kinetic energy can be decomposed into a linear flow energy and a linear heat. For highly non-equilibrium situations, temperature does not have a standard definition; however, kinetic energy and rms emittance do. As can be seen in Appendix B, rms emittance conservation occurs for non-interacting, non-relativistic adiabatic expansion, which is common place in accelerator physics. Furthermore, we showed that the mathematical formalism presented in this work can be extended to describe non-interacting relativistic dynamics and non-relativistic interacting systems in a straightforward manner. We will show in future work that relativistic interacting dynamics can likewise be explained using this formulation. Therefore, this relation between rms emittance and what we termed the linear heat, which can be thought of as the kinetic energy left over once the flow energy has been approximated through linear regression, is of critical importance for understanding systems in UEM/UED and accelerator physics.

We believe that this relation between emittance and linear heat may be why many scholars have tried a thermodynamic interpretation of emittance; specifically, emittance has long been suggested as being related to entropy^{12,26–31}. However, we show in Appendix B that under near equilibrium conditions the emittance is neither intensive nor extensive; in contrast the entropy is extensive. This leads us to conclude that emittance and entropy are not directly related. Of course, if the adiabatic expansion is reversible, we'd see that both the emittance

and entropy are conserved, but this does not mean that emittance and entropy are the same thing. One way to see some difference is to examine the expansion of a spherically symmetric continuous Gaussian distribution. Prior to the emergence of the shock, which breaks the laminar assumption, such a distribution is in fact reversible; however, the emittance does in fact grow – if only from non-linear effects.

Similar arguments concerning the thermodynamic properties of emittance have previously been presented by Bernal³²; further, Bernal concluded that an understanding of the mechanisms involved in emittance change was needed to advance beyond the current phenomenological understanding. The statistical kinematic presentation of emittance change presented in Eq. (20) provides such an avenue for understanding such mechanisms as we have explicitly demonstrated in the planar symmetric. In the planar symmetric case, only global and stochastic non-linearities play a role. Additional mechanisms are present in higher dimensional problems, and we will examine such mechanisms in future works.

VIII. DATA AVAILABILITY

The data that support the findings of this study are available from the corresponding author upon reasonable request.

ACKNOWLEDGMENTS

This work was supported by NSF Grant numbers RC1803719 and RC108666. We thank Steve Lund for introducing us to the work of Sacherer. We thank Omid Zandi for helpful discussion concerning emittance growth relations with fluid techniques and entropy.

Appendix A: Mathematical details of emittance growth calculations

Denote the i^{th} particles position and velocity at time $t = 0$ by $x_{0,i}$ and $v_{0,i}$, respectively, and at time t by x_i and v_i , respectively. In the laminar planar model, the force on the i^{th} particle, F_i is constant, so assuming non-relativistic conditions, the i^{th} particle's acceleration, $a_i = \frac{F_i}{m}$, is also a constant. Thus the kinematic equations for the i^{th} particle are given by Eq. (45a). Notice that x_i , v_i , $x_{0,i}$, $v_{0,i}$, and a_i differ among the particles, i.e. they are values

of the random variables x , v , x_0 , v_0 , and a . Using this notation, we can write

$$x = x_0 + v_0 t + \frac{1}{2} a t^2 \quad (\text{A1a})$$

$$v = v_0 + a t \quad (\text{A1b})$$

to be the map between the random variables using the ensemble constants of $\frac{1}{2}$, t , and t^2 .

The map in Eq. (A1) can be used to determine the evolution of any statistic. For example, the evolution in the velocity variance can be written as

$$\begin{aligned} s_v^2 &= s_{v,v} \\ &= s_{v_0+at, v_0+at} \end{aligned} \quad (\text{A2})$$

The right hand side of this equation can be simplified using Eq. (29) giving

$$s_v^2 = s_{v_0}^2 + s_a^2 t^2 + 2s_{v_0,a} t \quad (\text{A3})$$

Analogously, subbing Eq. (A1) into Eq. (10) and simplifying with Eq. (29), we obtain

$$\begin{aligned} c^2 \epsilon_{x,p}^2 &= s_{x_0}^2 s_{v_0}^2 - s_{x_0,v_0}^2 \\ &\quad + 2(s_{x_0}^2 s_{v_0,a} - s_{x_0,v_0} s_{x_0,a}) t \\ &\quad + (s_{x_0}^2 s_a^2 - s_{x_0,a}^2 - s_{x_0,a} s_{v_0}^2 + s_{x_0,v_0} s_{v_0,a}) t^2 \\ &\quad + (s_{x_0,v_0} s_a^2 - s_{x_0,a} s_{v_0,a}) t^3 \\ &\quad + \frac{1}{4} (s_{v_0}^2 s_a^2 - s_{v_0,a}^2) t^4 \end{aligned} \quad (\text{A4})$$

The right hand side of this equation can be shown to be equivalent to the determinant of Eq. (47).

Appendix B: Emittance of a ideal monatomic gas in a cubic box at equilibrium

We first consider the emittance of an ideal gas in a box whose edges all have width Δx and whose volume is $V = (\Delta x)^3$. We assume that the gas is at equilibrium meaning that there is no correlation between any of the 6D dimensions, x , y , z , p_x , p_y , and p_z , the distribution and that the spatial dimensions are distributed uniformly, and the momentum distribution follows the Maxwell-Boltzmann distribution. Using the definition of emittance in Eq. (15), we obtain under these conditions

$$\epsilon_{x,p_x}^2 = \frac{1}{m^2 c^2} s_x^2 s_{p_x}^2 \quad (\text{B1})$$

If the three spatial dimensions, x , y , and z are equivalent as they are in a cubic box, $\frac{s_{p_x}^2}{2m} = \frac{k_B T}{2}$. Thus we may write

$$s_{p_x}^2 = mk_B T \quad (\text{B2})$$

in this case. Likewise, s_x^2 may be related to the volume, V , of a closed container; the exact expression depends on the geometry of the distribution. In a cubic box, $V = \Delta x^3$ with a uniformly distributed gas, $s_x = \frac{1}{\sqrt{12}} \Delta x$. Thus

$$s_x^2 = \frac{V^{2/3}}{12} \quad (\text{B3})$$

Thus, the emittance can be written as

$$\varepsilon_{x,p_x}^2 = \frac{1}{12} \frac{k_B T}{mc^2} V^{2/3} \quad (\text{B4})$$

So, we see that emittance is proportional to the product volume raised to the $2/3$ power and temperature in a thermalized cubic box.

In the language of thermodynamics, temperature is intensive while volume is extensive, so emittance is neither intensive nor extensive, but a combination of intensive and extensive properties. In contrast, entropy is extensive. This has been pointed out previously by Bernal in his excellent paper arguing why the free energy model of emittance growth is problematic³². However, to students of thermodynamics, the product $TV^{2/3}$ should be familiar for another reason — it is the conserved quantity during the adiabatic expansion of an ideal monoatomic gas under non-relativistic conditions.

REFERENCES

- ¹B. J. Siwick, J. R. Dwyer, R. E. Jordan, and R. J. Dwayne Miller, *Journal of Applied Physics* **92**, 1643 (2002).
- ²B. W. Reed, *Journal of Applied Physics* **100**, 034916 (2006).
- ³B. Zerbe, X. Xiang, C.-Y. Ruan, S. Lund, and P. Duxbury, *Physical Review Accelerators and Beams* **21**, 064201 (2018).
- ⁴K. Huang, *Statistical mechanics 2nd edn* (Wiley, New York, 1987).
- ⁵M. Kardar, *Statistical physics of particles* (Cambridge University Press, 2007).
- ⁶A. Papoulis, *New York* **19842**, 115 (1991).

- ⁷M. Reiser, *Theory and Design of Charged Particle Beams* (John Wiley & Sons, New York, 1994).
- ⁸J. Buon, *Beam phase space and emittance*, Tech. Rep. (Paris-11 Univ., 1992).
- ⁹O. J. Luiten, S. B. vanderGeer, M. J. deLoos, F. B. Kiewiet, and M. J. vanderWiel, Physical review letters **93**, 094802 (2004).
- ¹⁰B. Reed, M. Armstrong, N. Browning, G. Campbell, J. Evans, T. LaGrange, and D. Masiel, Microscopy and microanalysis **15**, 272 (2009).
- ¹¹J. Lawson, in *AIP Conference Proceedings*, Vol. 253 (American Institute of Physics, 1992) pp. 1–10.
- ¹²P. M. Lapostolle, IEEE Transactions on Nuclear Science **18**, 1101 (1971).
- ¹³F. J. Sacherer, IEEE Transactions on Nuclear Science **18**, 1105 (1971).
- ¹⁴S. S. Wilks, Biometrika , 471 (1932).
- ¹⁵T. Wangler, K. Crandall, R. Mills, and M. Reiser, IEEE Transactions on Nuclear Science **32**, 2196 (1985).
- ¹⁶I. Hofmann and J. Struckmeier, Part. Accel. **21**, 69 (1986).
- ¹⁷T. P. Wangler, *Emittance growth from space-charge forces*, Tech. Rep. (Los Alamos National Lab., NM (United States), 1991).
- ¹⁸O. Anderson, Part. Accel. **21**, 197 (1987).
- ¹⁹J. Struckmeier, Part. Accel. **45**, 229 (1994).
- ²⁰J. Struckmeier, Physical Review Special Topics-Accelerators and Beams **3**, 034202 (2000).
- ²¹R. L. Gluckstern, Physical review letters **73**, 1247 (1994).
- ²²T. Wangler, K. Crandall, R. Ryne, and T. Wang, Physical review special topics-accelerators and beams **1**, 084201 (1998).
- ²³L. Serafini and J. B. Rosenzweig, Physical Review E **55**, 7565 (1997).
- ²⁴J. Rosenzweig, A. Cook, R. England, M. Dunning, S. Anderson, and M. Ferrario, Nuclear Instruments and Methods in Physics Research Section A: Accelerators, Spectrometers, Detectors and Associated Equipment **557**, 87 (2006).
- ²⁵J. Lawson, P. Lapostolle, and R. Gluckstern, Part. Accel. **5**, 61 (1973).
- ²⁶J. Struckmeier, Physical Review E **54**, 830 (1996).
- ²⁷N. Brown, Part. Accel. **56**, 51 (1996).
- ²⁸N. A. Brown, G. H. Gillespie, and B. W. Hill, in *Proceedings of the 1997 Particle Accelerator Conference (Cat. No. 97CH36167)*, Vol. 2 (IEEE, 1997) pp. 1894–1896.

- ²⁹P. G. OShea, in *AIP Conference Proceedings*, Vol. 377 (American Institute of Physics, 1996) pp. 309–321.
- ³⁰P. G. OShea, *Physical Review E* **57**, 1081 (1998).
- ³¹O. Boine-Frankenheim, I. Hofmann, J. Struckmeier, and S. Appel, *Nuclear Instruments and Methods in Physics Research Section A: Accelerators, Spectrometers, Detectors and Associated Equipment* **770**, 164 (2015).
- ³²S. Bernal, in *Proceedings of the Inter. Part. Accel. Conf.* (2015) p. MOPMA045.
- ³³I. Kapchinskij and V. Vladimirkij, CERN, Scientific Information Service, Geneva , 274 (1959).
- ³⁴A. Michalik and J. Sipe, *Journal of applied physics* **99**, 054908 (2006).
- ³⁵A. Michalik and J. Sipe, *Journal of Applied Physics* **105**, 084913 (2009).
- ³⁶J. A. Berger and W. A. Schroeder, *Journal of Applied Physics* **108**, 124905 (2010).
- ³⁷D. M. Lane, D. Scott, M. Hebl, R. Guerra, D. Osherson, and H. Zimmer, “Introduction to statistics, online edition,” (2017).
- ³⁸B. S. Zerbe and P. M. Duxbury, *Physical Review Accelerators and Beams* **22**, 114402 (2019).
- ³⁹B. S. Zerbe and P. M. Duxbury, *International journal of modern physics A* **34**, 1942042 (2019).
- ⁴⁰M. Bassetti and G. A. Erskine, *Closed expression for the electrical field of a two-dimensional Gaussian charge*, Tech. Rep. No. CERN-ISR-TH/80-06. (CERN, 1980).
- ⁴¹J. A. Berger, J. T. Hogan, M. J. Greco, W. A. Schroeder, A. W. Nicholls, and N. D. Browning, *Microscopy and Microanalysis* **15**, 298 (2009).
- ⁴²A. Gahlmann, S. T. Park, and A. H. Zewail, *Physical Chemistry Chemical Physics* **10**, 2894 (2008).
- ⁴³M. S. Robinson, P. D. Lane, and D. A. Wann, *Review of Scientific Instruments* **86**, 013109 (2015).
- ⁴⁴J. Maxson, I. Bazarov, W. Wan, H. Padmore, and C. Coleman-Smith, *New Journal of Physics* **15**, 103024 (2013).